Cell-type- and chromosome-specific chromatin landscapes and DNA replication programs of *Drosophila* testis tumor stem cell–like cells

Jennifer A. Urban, Daniel Ringwalt, John M. Urban, et al.

Genome Res. 2026 36: 83-101 originally published online December 10, 2025
Access the most recent version at doi:10.1101/gr.280809.125

Cell-type- and chromosome-specific chromatin landscapes and DNA replication programs of *Drosophila* testis tumor stem cell–like cells

Jennifer A. Urban,[1] Daniel Ringwalt,[1] John M. Urban,[2,3] Wingel Xue,[1,5] Ryan Gleason,[1] Keji Zhao,[4] and Xin Chen[1,2]

[1]*Department of Biology, The Johns Hopkins University, Baltimore, Maryland 21218, USA;* [2]*Howard Hughes Medical Institute, Baltimore, Maryland 21218, USA;* [3]*Biosphere Sciences and Engineering, Carnegie Institution for Science, Baltimore, Maryland 21218, USA;* [4]*Systems Biology Center, National Heart, Lung, and Blood Institute, National Institutes of Health, Bethesda, Maryland 20892, USA*

Stem cells have the unique ability to self-renew and differentiate into specialized cell types. Epigenetic mechanisms, including histones and their post-translational modifications, play a crucial role in regulating programs integral to a cell's identity, like gene expression and DNA replication. However, the transcriptional, chromatin, and replication timing profiles of adult stem cells in vivo remain poorly understood. Containing germline stem cells (GSCs) and somatic cyst stem cells (CySCs), the *Drosophila* testis provides an excellent in vivo model for studying adult stem cells. However, the small number of stem cells and the cellular heterogeneity of this tissue have limited comprehensive genomic studies. In this study, we develop cell-type-specific genomic techniques to analyze the transcriptome, histone modification patterns, and replication timing of germline stem cell (GSC)–like and somatic cyst stem cell (CySC)–like cells. Single-cell RNA sequencing validates previous findings on GSC–CySC intercellular communication and reveals a high expression of chromatin regulators in GSC-like cells. To characterize chromatin landscapes, we develop a cell-type-specific chromatin profiling assay to map H3K4me3-, H3K27me3-, and H3K9me3-enriched regions, corresponding to the euchromatic, facultative heterochromatic, and constitutive heterochromatic domains, respectively. Finally, we determine cell-type-specific replication timing profiles, integrating our in vivo data sets with published data using cultured cell lines. Our results reveal that GSC-like cells display a distinct replication program, compared with somatic lineages, that aligns with chromatin state differences. Collectively, our integrated transcriptomic, chromatin, and replication data sets provide a comprehensive framework for understanding genome regulation differences between these in vivo stem-cell populations, demonstrating the power of multiomics in uncovering cell-type-specific regulatory features.

[Supplemental material is available for this article.]

Stem cells are defined by their ability to self-renew and differentiate into specialized cell types. During development and tissue homeostasis, asymmetric cell division of stem cells produces two genetically identical daughter cells that adopt distinct cell fates. It is hypothesized that asymmetric inheritance of cell fate determinants plays a critical role in specifying these identities. Epigenetic mechanisms, such as histones and their post-translational modifications, regulate chromatin compaction, transcription, and DNA replication timing to influence cell fate decisions. In stem cells, epigenetic regulation is thought to be a key contributor to their differentiation potential. However, its precise roles in in vivo stem-cell systems remain to be fully elucidated.

The *Drosophila* male germline is a well-established model for studying stem-cell biology with well-defined cell lineages and differentiation programs. GSCs reside near the stem-cell niche and undergo asymmetric cell divisions to generate a self-renewing GSC and a differentiating gonialblast (GB) (Fig. 1A; Fuller and Spradling 2007; Matunis et al. 2012). Concurrently, CySCs divide to produce a CySC and a cyst cell (CC) (Gönczy and DiNardo 1996; Cheng et al. 2011). The GB, encapsulated by two CCs, undergoes four mitotic divisions with incomplete cytokinesis, forming a 16-cell spermatogonial (SG) cyst that subsequently enters meiosis (Fig. 1A; Matunis et al. 2012).

Traditional genetic and cell biological approaches have provided key insights into lineage-specific differences between GSCs and CySCs. These lineages communicate through cell–cell adhesion molecules and signaling pathways to coordinate germline cyst differentiation to become mature sperm (Matunis et al. 2012). However, the cell heterogeneity and small number of stem cells in wild-type testis tissue have made it difficult to generate comprehensive cell-type-specific genomic data sets defining their global transcriptional, chromatin, and replication landscapes. To address this, we developed cell-type-specific genomic strategies for testicular stem cells derived from a tumor model, enabling a detailed analysis of their transcriptome, chromatin landscapes, and replication timing dynamics. This approach

[5]**Present address: Harvard Medical School, Boston, MA 02115, USA**
Corresponding authors: jenurbanphd@gmail.com, xchen32@jhu.edu
Article published online before print. Article, supplemental material, and publication date are at https://www.genome.org/cgi/doi/10.1101/gr.280809.125. Freely available online through the *Genome Research* Open Access option.

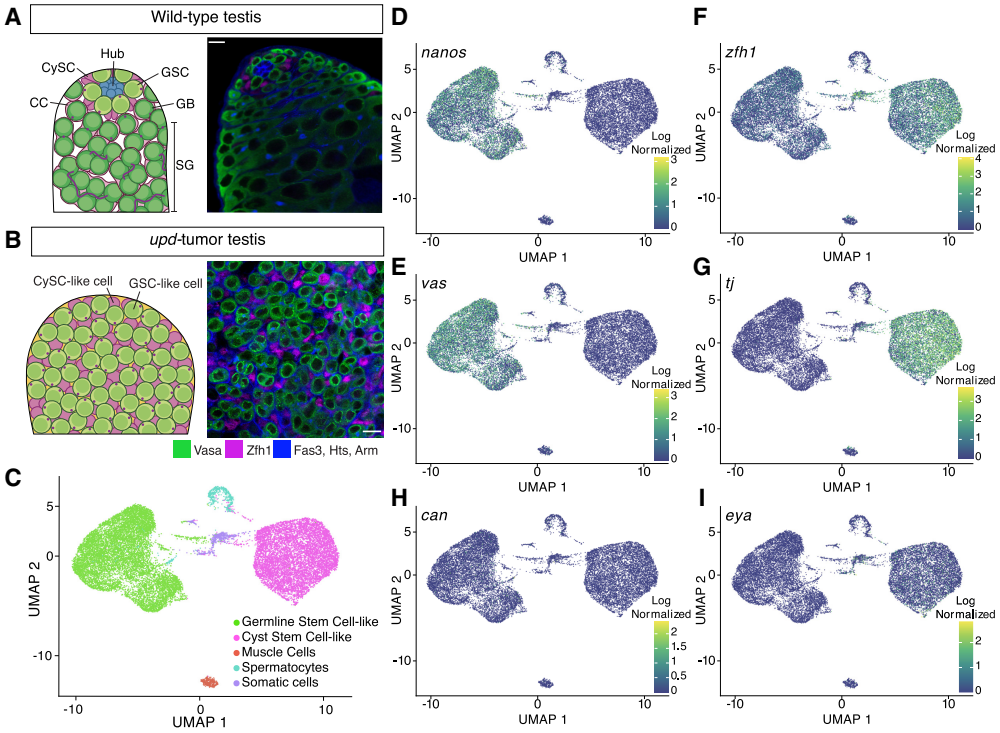

Figure 1. Single-cell RNA sequencing of *upd* tumor testes classifies two stem-cell populations. (*A*) Schematic of a wild-type testis alongside a single z-slice confocal image demonstrating the differentiation process of germline cells (green; Vasa-positive) and cyst cells (magenta; Zfh1-positive). At the apical tip, GSCs and CySCs surround the stem-cell niche, called the hub (Fas3; blue cell cluster). Individual spermatogonial (SG) cysts are identified by the spectrosome/fusome (Hts) and the extracellular adhesion protein, armadillo (Arm), both blue in the confocal image. Scale bar = 10 µm. (*B*) A schematic and single z-slice confocal image of the *upd* tumor. The tumor lacks a stem-cell niche and is composed of GSC-like (green; Vasa-positive) and CySC-like (magenta; Zfh1-positive) cells. In blue, is the cell adhesion protein armadillo (Arm) and the spectrosome (Hts), a spectrin-containing structure that appears as a dot in the cytoplasm of GSCs. The Vasa-positive, spectrosome-containing germline cells in the *upd* tumor display a morphology that is consistent with wild-type GSCs. Scale bar = 10 µm. (*C*) The *upd* tumor is composed of approximately five cell clusters, with the two largest groups representing GSC-like and CySC-like cells. (*D–I*) Uniform manifold approximation projection (UMAP) graphs show the cell- and stage-specific log-normalized expression of known marker transcripts that accurately define the GSC-like and CySC-like clusters.

uncovered previously unrecognized chromosome-specific differences in chromatin regulation between GSCs and CySCs, shedding new light on the molecular mechanisms regulating stem-cell identity and activity.

Results

Using a GSC and CySC tumor model for genomic studies

Our understanding of the transcriptional, chromatin, and replication landscapes of *Drosophila* GSCs is limited owing to their small number in wild-type testes (Fig. 1A; Supplemental Fig. S1A). GSCs were underrepresented in previous bulk genomic analyses of wild-type or early-stage germ-cell-enriched testes (Gan et al. 2010; Vedelek et al. 2018). Furthermore, even single-cell (single-cell RNA sequencing [scRNA-seq]) or single-nucleus (single-nucleus RNA sequencing [snRNA-seq]) transcriptomic methods using whole wild-type testes yielded sparse GSC data (Witt et al. 2019; Shi et al. 2020; Raz et al. 2023; Yu et al. 2023).

To overcome this limitation, we used testes enriched with GSC-like and somatic CySC-like cells by overexpressing the Janus kinase (JAK)–signal transducer and activator of transcription (STAT) pathway ligand unpaired (Upd) (Fig. 1B; Supplemental Fig. S1B). Hyperactivation of the JAK-STAT pathway in the testis results in overproliferation of both stem-cell types (Kiger et al. 2001; Tulina and Matunis 2001; Leatherman and DiNardo 2010), resulting in a more homogenous tissue composition for genomic profiling of stem cells from both germline and somatic lineages.

In our experimental design, we used two different cell-type-specific drivers to overexpress Upd in the fly testes. Driving expression of Upd with either a germline (*nanos* or *nanos*-Gal4) or somatic driver (*traffic jam* or *tj*-Gal4) leads to testis tumors with overproliferative GSC-like and CySC-like cells. A GFP-tagged histone H3 (H3-GFP) was driven along with Upd in either GSC-like cells (*nanos > upd*, *H3-GFP*) or CySC-like cells (*tj > upd*, *H3-GFP*). This tumor model reduces cellular heterogeneity, making it an ideal system for studying GSC- or CySC-specific transcriptional, chromatin, and replication landscapes.

scRNA-seq profiling of GSC-like and CySC-like cells

We performed scRNA-seq on *nanos*- and *tj*-driven Upd-overexpressing tumor samples (*upd* tumors), with two replicates each. Across these four samples, we consistently identified distinct germline and somatic lineages, demonstrated through single-cell integration, principal component analysis (PCA), and clustering (Supplemental Fig. S1C–E).

After individually clustering each sample, we integrated them to reduce batch effect variance and subset the data to GSC-like and CySC-like clusters. Consequently, most cells are clustered into two

Table 1. Composition and function of select DNA replication and chromatin regulation complexes

Complex name	Component names	Function
Origin recognition complex	**Orc1**, **Orc2**, Orc3, **Orc4**, **Orc5**, Orc6	Binds to origins of DNA replication
Minichromosome maintenance complex	**Mcm2**, **Mcm3**, **dpa**, **Mcm5**, Mcm6, **Mcm7**, **Mcm10**	DNA helicase unwinds dsDNA
Replication factors	Cdc45, dup, **geminin**, **cdc6**	Factors regulating initiation of the replisome
Replication Protein A	RPA1, RPA2, RPA3	Binds to single stranded DNA
DNA polymerase epsilon	**Chrac-14**, PolE1, **PolE2**, PolE4	Synthesizes leading strand DNA
DNA polymerase alpha	**PolA1**, **PolA2**, **Prim1**, **Prim2**	Synthesizes the RNA primer that initiates DNA synthesis
DNA polymerase delta	**PolD1**, **PolD2**, PolD3	Synthesizes lagging strand DNA
Other DNA polymerases	PolH, PolZ1, PolZ2, PolI, PolG1, PolG2, PolQ	Varied polymerases for DNA repair and mitochondrial DNA synthesis
Replication factor C/Egl1 complex	CG8142, **elg1**, **RfC3**, **RfC4**, **RfC38**	Regulates chromatin association of PCNA
DNA ligases	**DNAlig1**, DNAlig3, DNAlig4	Joins DNA strands
DNA Helicases	Dna2, **RecQ4**, RecQ5, Pif1	DNA helicases functioning in DNA repair
DNA *N*-glycosylases	Tdg, Ogg1, Nthl1	Enzymes that remove damaged bases from DNA
DNA polymerase Rev1	**Rev1**	DNA polymerase involved in translesion synthesis
DNA repair	**Brca2**	Involved in DNA repair
Chromatin assembly factor 1	Caf1-180, **Caf1-105**, Caf1-55	Assembles nucleosomes on newly synthesized DNA
Chromatin Accessibility Complex	**Acf**, **Chrac-14**, Chrac-16, Iswi	Regulates chromatin accessibility through nucleosome sliding
Histone variants	His4r, **Cid**, **His2Av**	Histone variants
Histone chaperones	Hira, Nap1	Histone chaperones
Nucleosome remodeling factor	Nurf-38, Caf1-55, E(bx), Iswi	Nucleosome sliding complex regulates accessibility for transcription
Remodeling and spacing factor complex	CG8677, Iswi	Remodeling and spacing factor complex
SNF2-like chromatin remodelers and NuRD	Mi-2, dom, chd3	Disrupts DNA–histone interactions
FACT	**dre4**, **Ssrp**	Interacts with H2A-H2B dimers and facilitates nucleosome formation

Components in bold are differentially enriched in GSC-like cells.

groups: GSC-like cells (expressing *vasa* and *nanos*) or CySC-like cells (expressing *tj* and *zfh1*) (Fig. 1C–G; Supplemental Table S1). Beyond these two main clusters, we identified three additional clusters: primary spermatocytes (*mst87f*-expressing), muscle cells (*act57B*-expressing), and an unidentified *wb*-expressing somatic lineage (Fig. 1C; Supplemental Fig. S1H; Supplemental Table S1; Kuhn et al. 1991; Kelly et al. 2002). For this study, we focus on the GSC-like and CySC-like clusters.

The GSC-like and CySC-like clusters followed expected gene expression patterns for known cell-type- and stage-specific markers. For example, GSC-like cells, but not CySC-like cells, express *nanos* and *vasa* (Fig. 1D,E; Supplemental Table S1). In contrast, CySC-like cells, but not GSC-like cells, express *zfh1* and *tj* (Fig. 1F,G; Supplemental Table S1).

The expression of stage-specific transcripts further confirms that the *upd* tumor is enriched with stem cell–like germline and cyst cells. As expected, *stat92E* is detected in both clusters, indicating JAK-STAT pathway activation is owing to *upd* overexpression (Supplemental Fig. S1I; Supplemental Table S1; Amoyel and Bach 2012). Additionally, as expected for GSCs, neither *bag of marbles* (*bam*), which is a marker of spermatogonia, nor *cannonball* (*can*), a spermatocyte-specific transcript, are strongly expressed in the GSC-like cell cluster (Fig. 1H; Supplemental Fig. S1I; Supplemental Table S1; McKearin and Spradling 1990; Hiller et al. 2001). Consistently, *eyes absent* (*eya*), a late-stage CC marker, is not expressed in the CySC-like cell cluster (Fig. 1I; Supplemental Table S1; Fabrizio et al. 2003).

We next compared our scRNA-seq data to published snRNA-seq from whole wild-type testes to investigate whether our results are consistent with the cell clusters identified in the published data set (Li et al. 2022; Raz et al. 2023). Our analysis confirms that GSC-like cells from the *upd* tumor are transcriptionally comparable to the wild-type cluster containing GSCs and early spermatogonia (Supplemental Fig. S2). Similarly, CySC-like cells show transcriptional similarity to the annotated CySC cluster in the published data set (Supplemental Fig. S2). These comparisons support our conclusion that the two major clusters from the *upd* tumor correspond to GSCs and CySCs, expressing characteristic cell-type- and stage-specific transcripts. The size and purity of these clusters provide an opportunity to robustly profile the transcriptomes of GSC- and CySC-like cells.

CySC-like cells highly express intercellular communication genes, whereas GSC-like cells enrich for chromatin regulators

To identify cell-type-enriched transcripts, we performed differential gene expression analysis. A transcript was considered as having significantly higher expression in GSC-like cells if it had a fold

change greater than 1.5 (GSC/CySC) and an S-value < 10^{-4} (estimated false sign rate) (Fig. 2A; Supplemental Table S2). We identified 827 genes enriched in GSC-like cells and 1794 in CySC-like cells. These GSC-like and CySC-like enriched gene sets contained expected markers, supporting cluster identity and the robustness of our analysis (Fig. 2B; Supplemental Table S2). First, the long noncoding RNAs (lncRNAs), *long non-coding RNA on the X 1* (*lncRNA:roX1*) and *lncRNA:roX2*, components of the male dosage compensation complex found in somatic but not germ cells (Shevelyov et al. 2022), rank among the top 100 genes with significantly higher expression in CySC-like cells (Fig. 2B; Supplemental Table S2). Second, *ago3*, encoding a germline-specific Argonaute required for piRNA-mediated transposon repression (Williams and Rubin 2002), is among the top 200 genes with significantly higher expression in GSC-like cells (Fig. 2B; Supplemental Table S2).

We performed Gene Ontology (GO) analysis to compare gene functions of expressed genes in GSC-like and CySC-like cells. We first analyzed the top 500 expressed transcripts based on their counts-per-million (CPM) values (top ~2.8%). We chose this approach to complement our differential gene expression analysis to address the limitation that genes expressed at similar levels in both cell types would otherwise be undetected. In this way, we found that CySCs are enriched with transcripts encoding cell–cell adhesion molecules and signaling pathway components at high levels (Fig. 2C; Supplemental Table S3). For example, the Cadherin-N (*cadN*) transcript level in the CySC-like cells (256.04 CPM) was higher than in the GSC-like cells (0.17 CPM) (Supplemental Table S1). Components from several signaling pathways, including the ErbB, epidermal growth factor (EGF), Hippo, Wnt, and Notch pathways, were identified as expressed highly in CySC-like cells (Fig. 2C; Supplemental Table S3), consistent with their roles in regulating CySC fate specification, division, and germline cyst enclosure (Kiger et al. 2000; Schulz et al. 2002; Parrott et al. 2012; Hudson et al. 2013; Ng et al. 2019). We also performed GO analysis on the 1794 significantly higher differentially expressed transcripts in CySCs. These transcripts are also enriched for genes involved in intercellular communication, including paracrine signaling pathway components and adhesion proteins (Fig. 2E; Supplemental Fig. S3A; Supplemental Table S3). For example, non-cell-autonomous bone morphogenic protein (BMP) signaling in somatic gonadal cells is essential for GSC maintenance and differentiation (Shivdasani and Ingham 2003; Kawase et al. 2004; Leatherman and DiNardo 2010). Components of this pathway, including the receptor thickveins (Tkv) and the ligands decapentaplegic (Dpp) and glass bottom boat (Gbb), are significantly higher expressed in CySC-like cells in our analysis (Supplemental Table S2). Together, these profiles align with the known supportive roles of somatic gonadal cells in spermatogenesis.

In contrast to CySC-like cells, the GO analysis of transcripts in GSC-like cells indicates the top 500 genes expressed in GSC-like cells are primarily chromatin regulators, such as the Facilitates Chromatin Transcription (FACT), Imitation Switch (ISWI), and Brahma complexes (Fig. 2D; Supplemental Table S3; Tyagi et al. 2016; Formosa and Winston 2020; Hu et al. 2021). For example, FACT complex subunits were expressed approximately five times higher in GSCs than in CySCs (Supplemental Table S1). We next examined the 827 significantly higher differentially expressed genes (DEGs) in the GSC-like cell cluster. The GSC-like transcriptome is differentially enriched for protein complexes involved in chromatin regulation, such as DNA replication, heterochromatin maintenance, and chromatin accessibility (Fig. 2F,G; Supplemental Fig. S3B–D; Table 1; Supplemental Table S3). Further, several chromatin-associated complexes contain multiple components, all significantly differentially expressed in GSC-like cells (Table 1). For example, genes encoding both FACT complex subunits, five minichromosome maintenance 2–7 (MCM2-7) complex components, and four origin recognition complex (ORC) components are all enriched in GSC-like cells compared with CySC-like cells (Table 1).

To control for potential biases in cell cycles, we normalized transcript representation across the G_1, S, and G_2/M cell-cycle phases such that both cell types have equivalent percentages of cells in each stage (33% G_1, 33% S, 33% G_2/M) (Supplemental Fig. S3F). This adjustment did not alter the enrichment pattern of genes, confirming that elevated replication gene expression in GSC-like cells reflects a true biological difference rather than differences in cell-cycle-phase distribution.

We next tested whether the enrichment of DNA replication factors detected in GSC-like cells from the *upd* tumor also occurs in GSCs from nontumor wild-type testes. Using genome editing, we generated knock-in fly lines with *gfp*-tagged endogenous *mcm2*, *orc1*, and *caf1-105*, genes considered differentially enriched in GSC-like cells (Fig. 2G; Table 1; Supplemental Fig. S3D). We then performed immunostaining on nontumor testes to examine the expression patterns of these GFP-fusion proteins and quantified GFP signals in wild-type GSCs and CySCs (Fig. 2H,I; Supplemental Fig. S3G). In all instances, normalized GFP signal was significantly higher in GSCs compared with CySCs (Fig. 2I), demonstrating that the protein levels in wild-type testes recapitulate the transcript enrichment identified in *upd* tumor samples. Together, these scRNA-seq data support the usage of *upd* tumor testes in uncovering key characteristics of wild-type stem cells through genomic strategies.

Cell-type-specific chromatin landscapes profiled by H3K4me3, H3K27me3, and H3K9me3

The high expression of chromatin regulators in GSC-like cells, revealed by our scRNA-seq analysis, suggests their potential roles in shaping distinct chromatin landscapes to regulate germline functions. This prompted us to investigate cell-type-specific chromatin patterns in GSC-like and CySC-like cells, respectively. To achieve this, we optimized a low-input cell-type-specific chromatin profiling method using *upd* tumor testes, which employs micrococcal nuclease (MNase) digestion of targeted chromatin (Fig. 3A). In this method, we coexpressed the Upd ligand and histone H3-GFP fusion protein in either GSC-like cells (*nanos* > *upd*, *H3-GFP*) or CySC-like cells (*tj* > *upd*, *H3-GFP*), as described earlier. MNase digestion specifically targeted chromatin containing H3-GFP using an anti-GFP antibody (Fig. 3A). After separating the soluble (GFP-containing) from insoluble (GFP-negative) chromatin, 5% of the soluble chromatin was sequenced as "input," whereas the remaining chromatin was prepared for low input chromatin immunoprecipitation (ChIP) sequencing (ChIP-seq) using antibodies against H3K4me3, H3K27me3, or H3K9me3 (Fig. 3A). We chose these histone modifications because they represent distinct chromatin domains: H3K4me3 (euchromatin), H3K27me3 (facultative heterochromatin), and H3K9me3 (constitutive heterochromatin) (Kouzarides 2007).

In agreement with previous findings (Kharchenko et al. 2011), H3K4me3 and H3K27me3 are enriched along the euchromatic chromosome arms but are depleted in the pericentromeric regions of Chromosomes 2, 3, and X (Fig. 3B; Supplemental Fig. S4A). In contrast, H3K9me3, which associates with constitutive

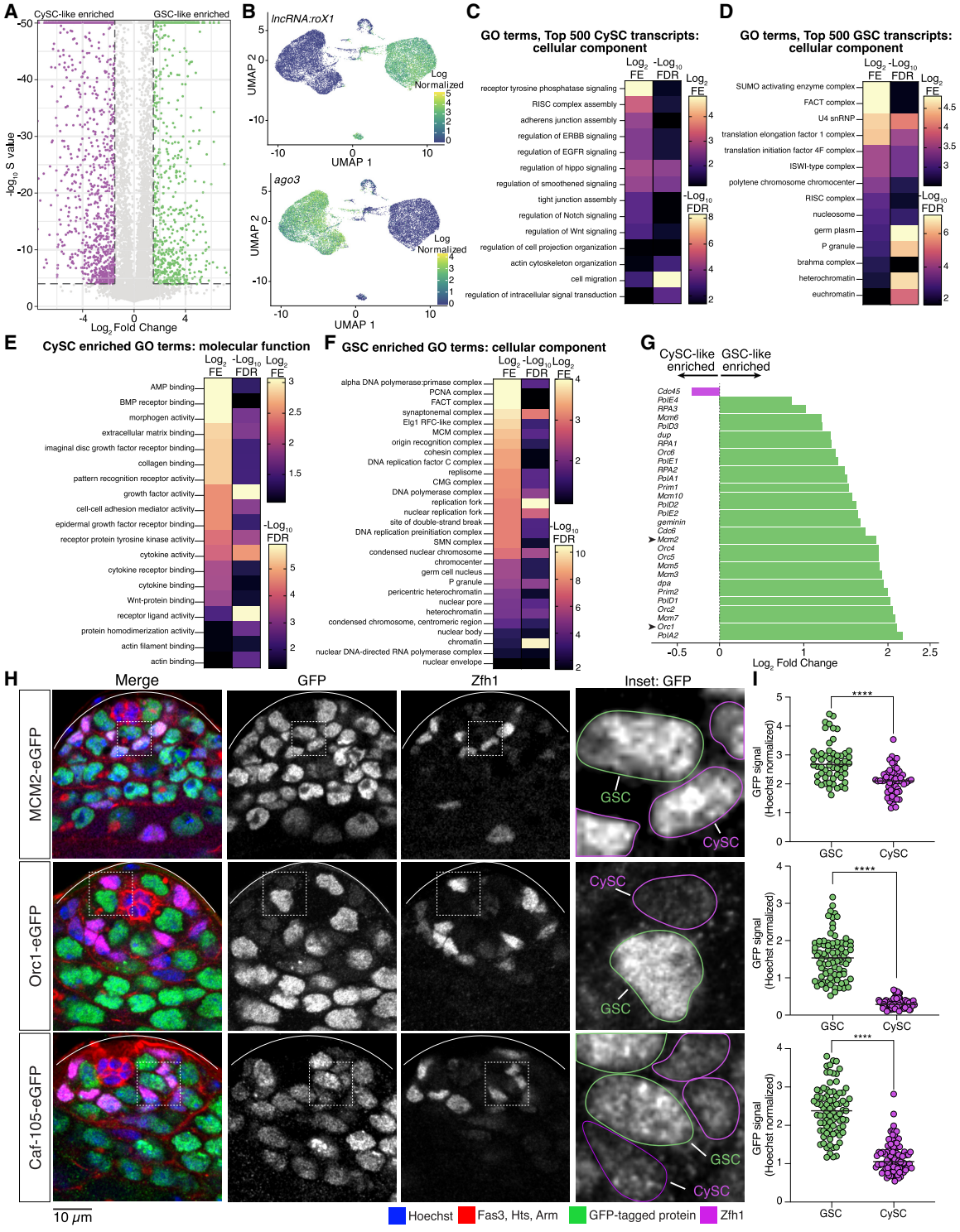

Figure 2. Intercellular communication in CySC-like cells and chromatin-based regulation in GSC-like cells. (*A*) Differential gene expression analysis between the transcriptomes of the GSC-like and CySC-like data sets. Differentially expressed transcripts are defined as having an absolute fold change difference >1.5 (GSC/CySC) and an estimated false sign rate (*S*-value) $< 10^{-4}$. (*B*) UMAP graphs of two known differentially expressed transcripts demonstrate the accuracy of cluster identification. *lncRNA:roX1*: $\log_2$ fold change (FC) = −6.01, *S*-value = 0; *ago3:* $\log_2$FC = 3.91, *S*-value = 0. (*C*,*D*) Gene Ontology (GO) analysis of the top 500 highest expressed genes in the CySC-like (at least 246.321917 CPM) and GSC-like (at least 258.44274 CPM) cell clusters. Shown are heatmaps of the $\log_2$ fold enrichment (FE) and negative $\log_{10}$ false-discovery rate (FDR) results from the GO analysis. (*E*,*F*) GO results for the significantly differentially expressed genes in CySC-like and GSC-like cells. Shown are heatmaps of the $\log_2$FE and negative $\log_{10}$FDR results from the GO analysis. (*G*) Differential transcript expression ($\log_2$ GSC/CySC) for select genes involved in DNA replication shows the higher expression of these genes in GSC-like cells (green bars). One gene, *Cdc45*, is differentially expressed in the CySC-like cells (magenta bar). (*H*) Confocal images of testis tips from fly strains with the indicated endogenously tagged GFP fusion protein. Expression of each protein is restricted within the mitotically active spermatogonial region. The *inset* displays a representative *z*-stack image outlining GSCs (in green) and CySCs (in magenta) that would be used for quantification. (*I*) The amount of GFP fluorescence within the volume of the nucleus of a GSC or CySC was normalized to the amount of Hoechst staining to produce the GFP signal value for that cell. The spectrosome, a germ-cell-specific organelle, and CySC-specific transcription factor Zfh1 were used to distinguish between GSCs and CySCs (Lin et al. 1994; Leatherman and DiNardo 2008). Two-tailed Mann–Whitney *U* test, (****) $P < 0.0001$.

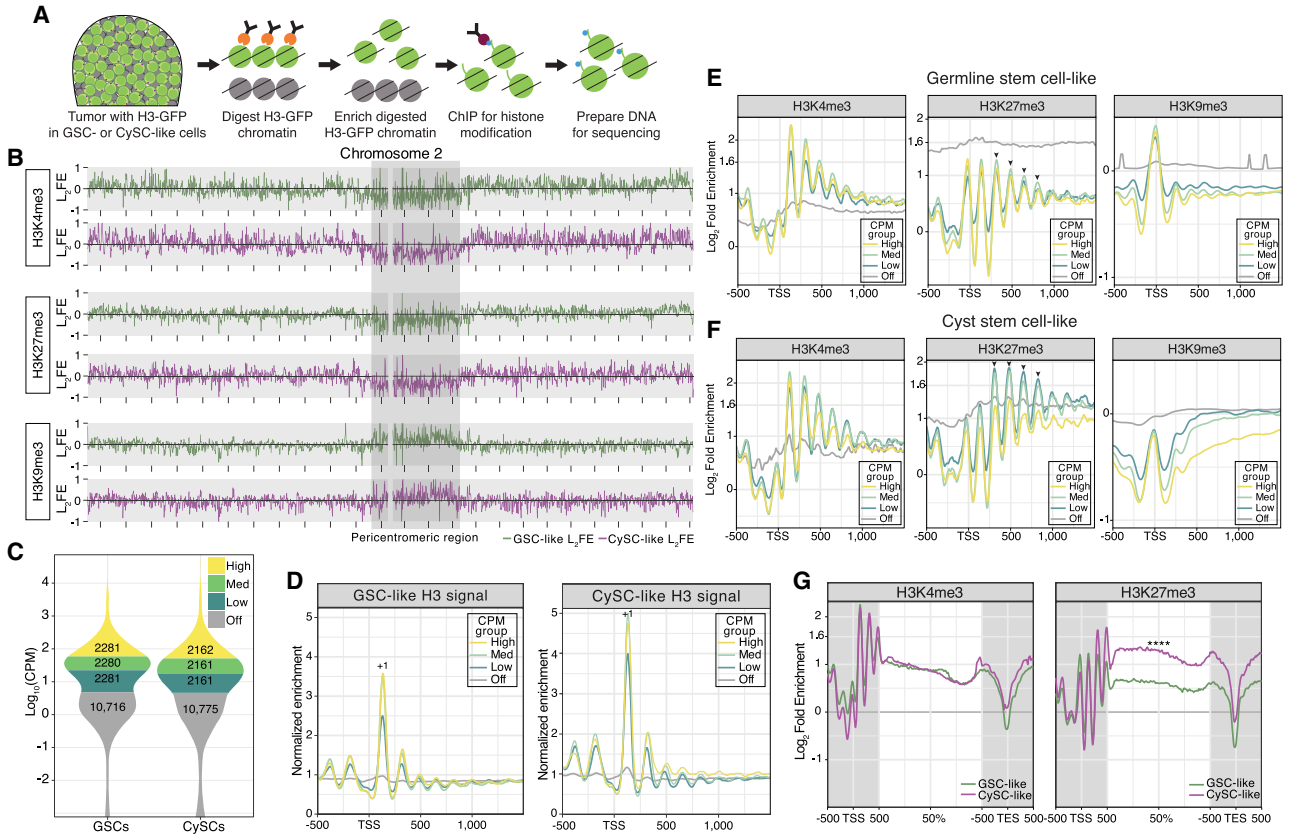

Figure 3. The cell-specific chromatin profiles of H3K4me3, H3K27me3, and H3K9me3. (*A*) Schematic of the cell-specific chromatin immunocleavage (ChIC) coupled with chromatin immunoprecipitation (ChIP) protocol. Chromatin containing a histone H3-GFP fusion protein is targeted for digestion by antibody-guided MNase. After enriching for digested chromatin, a low-input ChIP protocol is performed for either the H3K4me3, H3K27me3, or H3K9me3 chromatin modification. (*B*) The $\log_2$FE of H3K4me3, H3K27me3, and H3K9me3 along the euchromatic arms and pericentromeric region of Chromosome 2. Enrichment tracks from GSC-like cells are in green, whereas the tracks associated with CySC-like cells are in magenta. The distance between each mark along the *x*-axis is equivalent to 2 Mb. (*C*) Using a cut-off of CPM > 5 as "on," the transcriptomes of the GSC-like and CySC-like clusters obtained from the scRNA-seq were divided into three equal parts to define genes as either off, low, medium, or high expression. (*D*) Enrichment of mononucleosome fragments (as a density estimation of input monosomal fragment midpoints) is plotted at transcription start sites (TSSs) of genes separated by their expression level as defined in *C*. The normalized enrichment of mononucleosome fragments was determined by normalizing to the median mononucleosomal fragment count on autosomes. The +1 nucleosome is indicated in each graph. Enrichment at the maximum $\log_2$FE value was compared to the "off" gene value using a Welch's *t*-test for each CPM group, indicating a strong significant difference in fragment enrichment (Supplemental Table S4). (*E*,*F*) Cell-specific histone modification enrichment was calculated as the $\log_2$FE ($\log_2$[average mark signal/H3 (input) signal]) and then plotted at the TSS of genes categorized by their expression level. Arrowheads indicate the position of nucleosomes at which a difference in H3K27me3 enrichment is observed between the GSC-like and CySC-like chromatin profiles. As done earlier, enrichment at the maximum $\log_2$FE value for each CPM group was compared to the "off" gene value using a Welch's *t*-test, indicating a strong significant difference in modification enrichment (Supplemental Table S4). (*G*) Comparing the average gene profiles of $\log_2$FE along gene bodies between GSC-like and CySC-like cells shows no difference in enrichment for H3K4me3, but a Welch's *t*-test determined a significant increase in H3K27me3 enrichment in CySC-like cells (Supplemental Table S4).

heterochromatin, shows enrichment at pericentromeric regions (Fig. 3B; Supplemental Fig. S4A). Together, these results demonstrate that our cell-type-specific chromatin profiling assay accurately recapitulates chromatin signatures consistent with the known distributions of H3K4me3, H3K27me3, and H3K9me3 (Kharchenko et al. 2011).

To investigate relationships between chromatin patterns and cell-type-specific gene expression, we integrated our cell-type-specific chromatin profiles with the scRNA-seq results. Focusing on the GSC-like and CySC-like clusters, we defined a transcript as expressed ("on") if its CPM was above five, a threshold that reliably separates known cell-type-specific expressed genes from nonexpressed genes (CPM < 5, "off"). For example, using this cutoff, *ago3* is classified as "off" in the CySC-like cluster (CPM = 2.11) but is robustly expressed in the GSC-like cluster (CPM = 697.21) (Fig. 2B; Supplemental Table S1), indicating strong cell-type-specific expression (Williams and Rubin 2002). We further classified "on" genes into three categories based on their transcript levels: low, medium, and high (Fig. 3C). The GSC-like and CySC-like clusters contained similar numbers of "on" and "off" genes (GSCs: 6842 "on" and 10,716 "off"; CySCs: 6484 "on" and 10,775 "off"), whereas the remaining three smaller clusters displayed comparable numbers of "on" and "off" genes (Supplemental Fig. S4B).

Using these categories, we plotted mononucleosomal enrichment to understand how nucleosomal position and density influence gene expression. The phased distribution of the H3 signal, indicative of nucleosome positioning, displays the characteristic mononucleosomal pattern generated by the MNase (Fig. 3D). This approach reveals the strongly positioned +1 nucleosome near the transcription start sites (TSSs) of actively expressed genes in both cell types, with positioning strength diminishing as gene

expression levels decrease (Fig. 3D; Supplemental Table S4). This observation aligns with the known association between strongly positioned nucleosomes and chromatin organization at active genes, underscoring the role of nucleosome positioning in regulating gene expression and further validating our experimental approach (Chereji et al. 2018).

H3K27me3 plays a more prominent role in CySC-like cells compared with GSC-like cells

To investigate the relationship between histone modifications and gene expression, we analyzed enrichment of H3K4me3, H3K27me3, and H3K9me3 at TSS relative to transcript levels using input-normalized $\log_2$ fold enrichment ($\log_2$FE). In both GSC-like and CySC-like cells, H3K4me3 enrichment positively correlates with gene expression (Supplemental Fig. S4C,E). Consistently, average enrichment profiles show a pronounced H3K4me3 peak at the +1 nucleosome of expressed genes (Fig. 3E,F; Supplemental Table S4). In contrast, silenced genes display higher H3K9me3 enrichment compared with expressed genes (Fig. 3E,F; Supplemental Fig. S4C,E), with transposable elements having particularly strong enrichment, consistent with the role of H3K9me3 in marking constitutively repressed regions (Supplemental Fig. S4D; Supplemental Table S4). Because gene expression categories were defined independently for each cell type, we also compared average gene profiles of genes expressed in both cell types and uniquely in one versus the other (Supplemental Fig. S4F,G). The overall patterns of individual histone modifications were similar across gene sets, regardless of cell type, indicating that no single histone mark alone can predict cell-specific gene expression (Supplemental Fig. S4G).

Among the three profiled histone modifications, H3K27me3 displays distinguishable cell-type-specific differences between GSC-like and CySC-like cells, indicating potentially distinct roles for this modification in these two cell types (Supplemental Fig. S4C,E). In GSC-like cells, H3K27me3 shows moderate enrichment across all expressed gene categories (Fig. 3E; Supplemental Fig. S4C,E,G), whereas silenced genes display stronger enrichment despite lacking well-positioned nucleosomes (Fig. 3E). This noncanonical H3K27me3 enrichment resembles the pattern observed in female *Drosophila* GSCs, in which H3K27me3 is detectable at both inactive and active gene loci (DeLuca et al. 2020).

In contrast, in CySC-like cells, H3K27me3 is most enriched at the lowest-expressed genes and gradually decreases with increasing gene expression levels (Fig. 3F; Supplemental Fig. S4C,E). This H3K27me3 pattern is consistent with its well-established role in gene repression. Further, in CySC-like cells, H3K27me3 enrichment increases at the +3 nucleosome position and extends into the gene body for medium- and low-expression genes, a distinct feature not observed in GSC-like cells (Fig. 3E,F).

Previous studies demonstrate that broad H3K4me3 domains mark genes critical for cell identity and function in stem and progenitor cells. As cells differentiate and lose potency, these broad H3K4me3 domains become refined (Zhang et al. 2021). Further, broad H3K27me3 enrichment across gene bodies is associated with gene repression (Young et al. 2011). To investigate whether broad histone modification patterns are present in the two populations of stem cells in testis, we analyzed histone modification enrichment across the gene bodies in genes expressed in both GSC-like and CySC-like cells (Fig. 3G). Our analysis revealed similar H3K4me3 enrichment along the gene bodies in both cell types (Fig. 3G; Supplemental Table S4). However, H3K27me3 was significantly enriched along the gene bodies in CySC-like cells (Fig. 3G; Supplemental Table S4). This differential enrichment indicates a cell-type-specific regulatory mechanism for which H3K27me3 plays a more prominent role in CySC-like cells than in GSC-like cells.

Previous functional studies in *Drosophila* testes demonstrate that the histone methyltransferase Enhancer of zeste [E(z)], which generates H3K27me3, plays a critical non-cell-autonomous role in the CySC lineage by preventing ectopic expression of a key somatic transcription factor in germ cells (Eun et al. 2014). Conversely, inactivation of E(z) in the germline results in only mild defects, which arise in later-stage germ cells rather than in GSCs (Eun et al. 2017). This indicates H3K27me3 may not play a large role in the early germline. Consistent with these findings, our scRNA-seq data show moderate *E(z)* expression in both GSC-like (CPM = 74.33) and CySC-like (CPM = 20.89) cells (Supplemental Fig. S4H; Supplemental Table S1). However, transcript levels for *Utx*, the demethylase responsible for erasing the H3K27me3 modification, are more highly expressed in the GSC-like cluster (GSC-like CPM = 64.17; CySC-like CPM = 31.06) (Supplemental Fig. S4I; Supplemental Table S1). Together, these findings highlight a role for E(z) and H3K27me3 in the CySC lineage, in which they regulate the identity and activity of the GSC lineage in a non-cell-autonomous manner. Moreover, these data suggest a noncanonical H3K27me3 chromatin pattern in male GSC-like cells, resembling the pattern detected in female GSCs (DeLuca et al. 2020).

Distinct replication timing profiles in GSC-like and CySC-like cells

Chromatin organization plays an integral role in regulating transcription and DNA replication. Given the differences in chromatin landscapes between GSC-like and CySC-like cells, we aimed to understand how replication timing differs between these cell types using replication sequencing (Repli-seq) (Fig. 4A; Supplemental Fig. S5A–C; Marchal et al. 2018). First, we dissected *upd* tumors expressing H3-GFP in either GSC-like or CySC-like cells and incubated them with the thymidine analog bromodeoxyuridine (BrdU) to label replicating DNA. Next, GSC-like or CySC-like nuclei were extracted and sorted via flow cytometry into four S-phase fractions corresponding to early, early-mid, late-mid, and late S phase, based on their DNA content (Fig. 4A; Supplemental Fig. S5A–C). BrdU-labeled DNA was then immunoprecipitated, followed by library preparation and sequencing (Fig. 4A).

We generated replication timing profiles to identify early- and late-replicating genomic regions on each chromosome. In these profiles, enrichment of Repli-seq reads in the early fraction yields a positive score, just as late fraction enrichment yields a negative score. Consistent with known replication timing patterns, pericentromeric heterochromatin is largely late-replicating in both GSC-like and CySC-like cells (Fig. 4B,C). On the other hand, in both cell types, the chromosomal arms of Chromosomes 2, 3, and the X replicate throughout the S phase, with some regions replicating early and others late (Fig. 4B,C). The 2 and 3 Chromosomes comprise 70%–80% of the *Drosophila* genome and display distinct chromatin landscapes between the chromosome arms and pericentromeric regions (Fig. 3B; Supplemental Fig. S4A). To examine replication progression relative to these chromatin domains, we plotted replication timing values for these two major autosomes, separating the arms from the pericentromeric regions. Minimal replication timing differences were detected between GSC-like and CySC-like cells along the major autosomal arms (Fig. 4C). Notably, although pericentromeric regions for both major

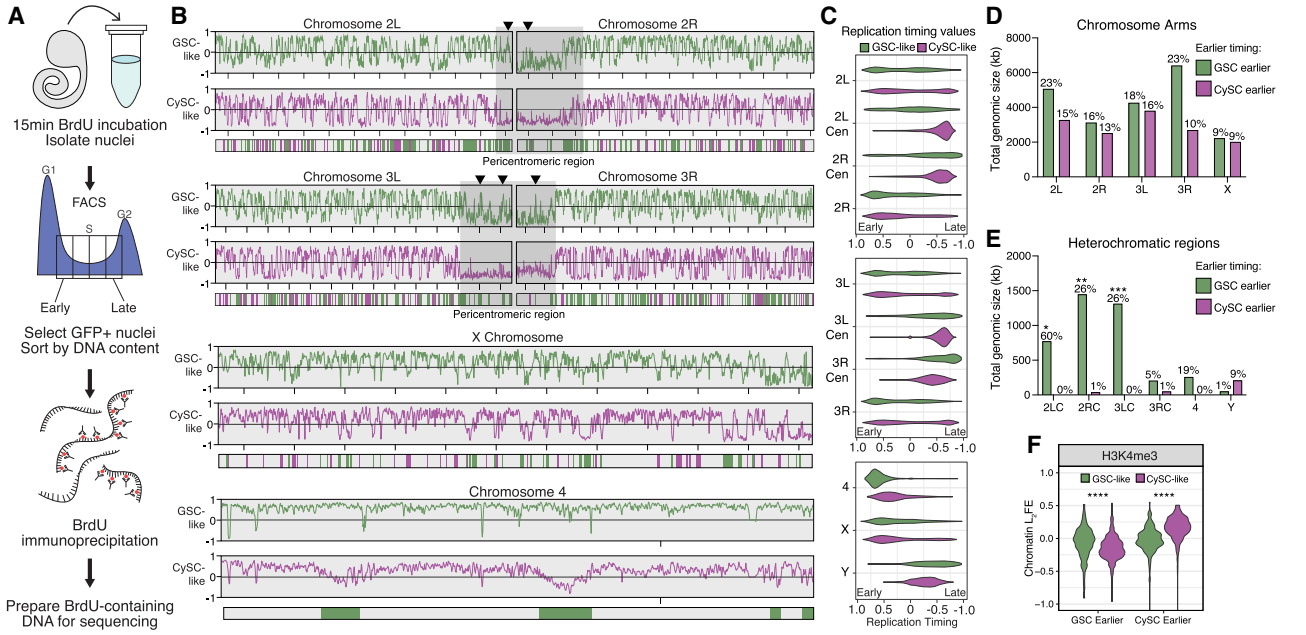

Figure 4. The replication timing profiles of GSC-like and CySC-like cells are distinct. (*A*) A schematic of the Repli-seq protocol. First, dissected *upd* tumors are incubated with BrdU, followed by nuclei isolation. GFP-positive nuclei are then sorted by DNA content, separating into one of four S-phase fractions: early, early-mid, late-mid, or late replicating. Next, the BrdU-containing DNA is immunoprecipitated and prepared for sequencing to identify genomic locations undergoing replication within the specific stages of S phase. (*B*) Replication timing is scored from −1 to 1, with positive values representing early replicating and negative values representing late replicating. Replication timing line plots for GSC-like (green) and CySC-like (magenta) are separated for each chromosome. *Below* the line plots are the genomic windows in which replication timing significantly differed between the GSC-like and CySC-like cells, for which the color indicates the cell type with earlier replication. Pericentromeric regions on Chromosomes 2 and 3 are indicated by gray boxes. Arrowheads denote example heterochromatic locations at which the GSC-like replication timing is significantly earlier than CySC-like cells. (*C*) The replication timing values for each chromosome are plotted as violin plots and separated by heterochromatic or euchromatic regions. A Welch's *t*-test of the logit-transformed violins indicated there is a significant difference in the replication timing values for all comparisons between GSC-like and CySC-like distributions, except the X Chromosome (Supplemental Table S5). (Cen) Pericentromeric heterochromatin. (*D*,*E*) Shown is the total genomic size in kilobases for each chromosome for which we rejected the null hypothesis of no difference in timing among GSC-like or CySC-like cells. In general, heterochromatic regions are earlier replicating in GSC-like cells. *Above* each bar is the percentage of the indicated chromosome that corresponds to the total genomic size that is earlier replicating. Statistical significance was determined by a Fisher's exact test with category aggregation of the chromosome regions (Supplemental Table S6). (*F*) The $\log_2$FE values for H3K4me3 are significantly elevated in regions that are cell-specifically earlier replicating. Statistical significance was determined by a paired-sample *t*-test (Supplemental Table S5).

autosomes were consistently late-replicating in CySC-like cells, they displayed early replication features in GSC-like cells (Fig. 4B, C; Supplemental Table S5). The fourth chromosome replicates early in GSC-like cells, despite its known heterochromatic nature (Fig. 4B,C; Haynes et al. 2007). Overall, GSC-like cells exhibited a trend in which traditionally heterochromatic regions replicate earlier than expected, suggesting previously unrecognized roles for these regions in regulating GSC functions.

We next compared replication timing values between GSC-like and CySC-like cells to identify genomic regions with significantly different timing regimes. Using 3 kb sliding windows, we tested the null hypothesis that replication timing is equal between the two stem-cell types. Nested peak calling was then performed to identify regions at least 20 kb in size with significant timing differences between the two cell types. Regions were then categorized as "GSC earlier" or "CySC earlier" depending on whether they replicate earlier in GSC-like or CySC-like cells (Fig. 4B; Supplemental Fig. S5D). Overall, 25.12 Mb of the genome replicates earlier in GSC-like cells compared with CySC-like cells, whereas 14.588 Mb replicates earlier in CySCs-like cells (Fig. 4D,E; Supplemental Table S6). In addition to total genomic size, we calculated the fraction of each chromosome that replicates earlier to gain perspective on the scale of these differences (Supplemental Table S6). The total genomic size of earlier replicating regions is similar between GSC-like and CySC-like cells across the major autosomal arms and the X Chromosome (Fig. 4D). A notable exception is the right arm of Chromosome 3, in which the total amount of kilobases replicating earlier in GSC-like cells is much greater than CySC-like cells. Accordingly, 23% of Chromosome 3R replicates earlier in GSC-like cells, whereas just 10% of this chromosome replicates earlier in CySC-like cells (Fig. 4D; Supplemental Table S6).

In heterochromatic regions, GSC-like cells exhibited a greater total genomic size of earlier-replicating DNA compared with CySC-like cells (Fig. 4E). These differences span substantial portions of the genome. For example, earlier-replicating domains in GSC-like cells account for 60% of the pericentromeric heterochromatin on Chromosome 2. A notable exception is the Y Chromosome, in which 9% of the Y Chromosome replicates earlier in CySC-like cells than in GSC-like cells (Fig. 4E; Supplemental Fig. S5D). To examine whether differences in replication timing align with differences in histone modification enrichment, we analyzed $\log_2$FE values from our cell-type-specific histone modification data. As expected, regions that replicate earlier in GSC-like cells show significantly greater H3K4me3 enrichment in this cell type (Fig. 4F; Supplemental Table S5). Similarly, earlier replicating regions in CySC-like cells are enriched for H3K4me3 in these cells (Fig. 4F; Supplemental Table S5). These results indicate that cell-type-specific replication timing differences align with cell-type-specific

chromatin features. For the first time, our results enable precise identification of specific chromosomal regions that differ in replication timing and chromatin landscapes between germline and somatic stem-cell populations in the in vivo context.

Replication timing of GSC-like cells is distinct from that of CySC-like and cultured *Drosophila* cells

Although most studies on replication timing have focused on cultured cell lines, studies using in vivo cells from a normal developmental context revealed differences in replication timing profiles during cell fate specification. This highlights how dynamic variations in replication programs associated with changes in cellular potency cannot be captured by studying cultured cells alone (Siefert et al. 2017; Armstrong et al. 2018; Das et al. 2021; Pratto et al. 2021; Nakatani et al. 2023; Takahashi et al. 2024). To gain cell-type-specific insights and compare replication timing between in vivo and in vitro cells, we compared our data sets with published replication timing data from two well-studied *Drosophila* cell lines, Kc167 and S2 (Lubelsky et al. 2014). Our analysis suggests that the replication timing profile of GSC-like cells is distinct from the other three cell types, whereas the two cell lines cluster together (Fig. 5A).

To facilitate cross-cell-type comparisons, we standardized replication timing along the reference genome to have unit variance, yielding RT *Z*-scores. We then categorized the genome into 12 chromosomal domains with their mean RT *Z*-scores: two major autosomal arms and their pericentromeric regions, the 4th, X, and Y Chromosomes, and a gene consensus for the ribosomal DNA (rDNA) locus (Fig. 5B). This allowed us to characterize negatively and positively correlated cell-type profiles (Supplemental Fig. S6A). Among the four cell types, GSC-like and Kc167 cells show the strongest correlation in their chromosomal region RT *Z*-score profiles (Supplemental Fig. S6A). This is intriguing because Kc167 cells are female (XX karyotype) (Cherbas and Gong 2014). Similarly, CySC-like and S2 cells display positively correlated RT *Z*-scores, likely owing to their shared somatic identity and male (XY) karyotype (Supplemental Fig. S6A).

We additionally summarized the chromosomal region RT *Z*-scores by their arithmetic mean (Fig. 5B). These summarized *Z*-scores, relative to the combined data set mean, indicate how each genomic region in each cell type deviates from the data set's average (Fig. 5B). Although chromosomal arms display no overall trends, this method identified earlier replication timing in GSC-like cells for the pericentromeric region of Chromosome 2L (early-mid), the fourth chromosome (early), and the rDNA locus (early) (Fig. 5B). Although replication timing for the X Chromosome was found to be early-mid and the Y Chromosome to be late-mid in both GSC-like and CySC-like cells (Supplemental Table S5), the *Z*-scores revealed more genomic regions on both sex chromosomes that replicate earlier in CySC-like cells (Fig. 5B). Intrigued by the early-replicating result at the rDNA locus, we plotted replication timing scores for each cell type across the 8 kb transcriptional unit within the rDNA locus in the dm6 genome. Indeed, although the negative replication timing values for CySC-like, Kc167, and S2 cells indicate late replication, positive values in GSC-like cells demonstrate their cell-type-specific early replication timing (Fig. 5C).

Pairwise comparisons of replication timing profiles across the four cell types identified genomic windows with distinct replication timing. As shown above, we quantified the total size (in kilobases) of earlier-replicating regions and mapped their genomic locations by cell type. Additionally, we calculated the corresponding proportion of each chromosomal domain that replicates earlier. The arms of the second and third chromosomes show minimal differences in the amount, proportion, or location of cell-type-specific earlier-replicating regions (Fig. 5D,E; Supplemental Fig. S6B, C). Thus, differences in replication timing are present across the chromosome arms and collectively encompass 12%–30% of these chromosome domains.

We next focused on regions where the mean RT *Z*-score suggests earlier replication in GSC-like cells, such as the pericentromeric region of Chromosome 2L and the fourth chromosome. In both cases, the total genomic size of earlier replicating regions is greater in GSC-like cells compared with other cell types (Fig. 5F, G; Supplemental Fig. S6D,E; Supplemental Table S6). The pericentromeric region does not have specific locations with significantly different replication timing between the GSC-like cells and other cell types; rather, the entire region displays earlier replication timing in GSC-like cells than in both CySC-like and S2 cells (Fig. 5F). Kc167 and GSC-like cells have comparable replication timing patterns within this region (Fig. 5F). In contrast to the pericentromeric region of Chromosome 2L, the fourth chromosome contains three distinct regions, accounting for ~19% of this chromosome, with comparatively earlier replication timing in GSC-like cells (Fig. 5G; Supplemental Fig. S6E).

The Y Chromosome generally replicates late in the S phase across all three male cell types (Fig. 5H). However, CySC-like cells show a relatively earlier replication timing profile, as reflected by their mean RT *Z*-score (Fig. 5B). Indeed, the total genomic size of earlier-replicating regions is larger in both CySC-like and S2 cells compared with GSC-like cells, whereas CySC-like and S2 cells show similar values (Fig. 5H; Supplemental Table S6). Unlike the fourth chromosome, replication timing for the Y Chromosome does not reveal any consistent earlier-replicating regions and these domains compose small fractions of the Y Chromosome (Fig. 5H). However, a few specific loci show different replication timing when comparing GSC-like to CySC-like cells, which are subject for subsequent analyses (Fig. 5H).

Finally, when comparing male cells (GSC-like, CySC-like, or S2) to female Kc167 cells, the X Chromosome consistently replicates earlier in the male cell, whereas the average replication timing of the X Chromosome was similar among male cell types (all with a summary RT value of 0.48 ± 0.01) (Fig. 5I; Supplemental Fig. S6F; Supplemental Table S5). This predominance of early replication of the X Chromosome in male cells likely reflects the accessible chromatin environment that facilitates male-specific X Chromosome dosage compensation (Urban et al. 2017). Early X Chromosome replication is preserved in GSC-like cells, despite the absence of dosage compensation in this cell type (Fig. 2D; Meiklejohn et al. 2011). Our scRNA-seq further supports this note, showing no evidence of X-linked gene dosage compensation in GSC-like cells or primary spermatocytes, based on the X-to-autosome (X:A) transcript abundance ratios (Supplemental Fig. S6G). Overall, our analysis identifies key genomic regions with cell-type-specific replication timing differences, including heterochromatic pericentromeric regions and the fourth chromosome and the X and Y Chromosomes, suggesting distinct functional requirements for these domains across different cell types.

Cell-type-specific replication timing correlates with histone modification patterns

The temporal order of genome duplication in eukaryotic cells is intricately linked to chromatin structure and gene expression, both

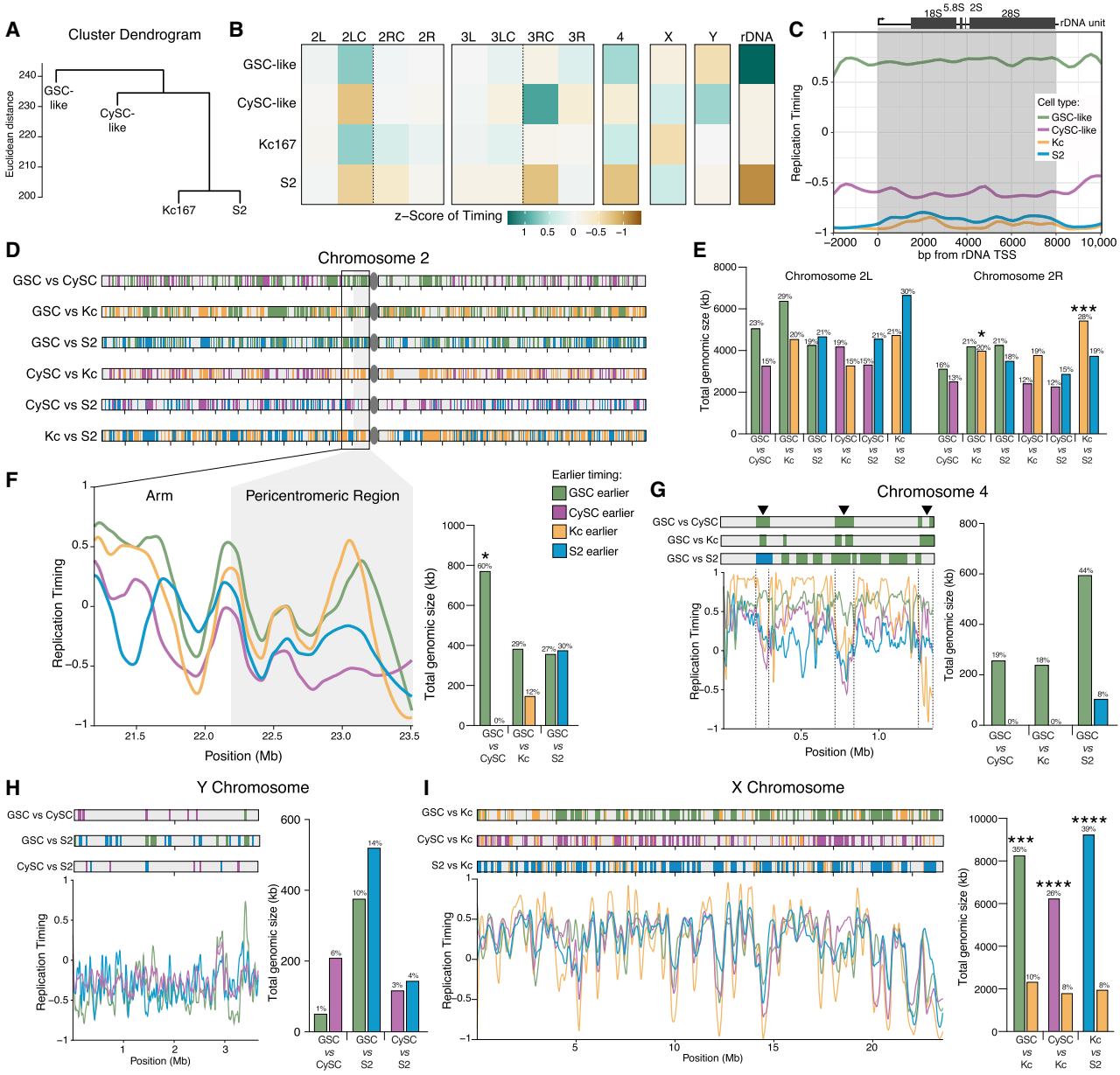

Figure 5. GSC-like cells have a distinct replication timing program from CySC-like and cultured *Drosophila* cells. (*A*) Hierarchical comparison of replication timing indicates that the GSC-like cell replication program is dissimilar to the other three replication programs. On the *y*-axis, tree branches are shown at the root mean squared *Z*-score difference of all genomic windows (Euclidean distance), and cell–cell distances at each tree branch are combined using the average method. (*B*) The mean replication timing *Z*-score for 11 defined chromosomal regions and the *Z*-score of the rDNA unit indicate how this summary of the genome hierarchically explains the cell types' epigenomes. (*C*) Plot of replication timing for each cell type across the 8 kb transcribed rDNA unit. Early replication timing for this genomic location only occurs in GSC-like cells. (*D*) Pairwise comparison of replication timing differences for Chromosome 2, in which domains (reaching a size at least 20 kb) are evaluated against the null hypothesis of having equal replication timing. Shown are the location and identification of regions that are replicating earlier in the indicated comparison. (*E*) The sum total genomic size of pairwise comparisons that are replicating earlier in the specified cell comparison for the left and right arms of Chromosome 2. Statistical significance for total genomic size was calculated using a Fisher's exact test with category aggregation of chromosomes (Supplemental Table S6). The total genomic size was divided by the length of each chromosome arm to calculate the fraction (in percentage) of the arm replicating earlier in that cell type. These values are shown *above* each bar. (*F*) Replication timing line plots for each cell type within the pericentromeric region of Chromosome 2 demonstrates the locations where the GSC-like cells replicate early in comparison to the other cell types. A quantification of the total genomic size at which GSC-like cells replicate earlier is presented on the *right* with the fraction of pericentromeric region that is earlier replicating presented *above* each bar. (*G*) The fourth chromosome has more genomic regions that replicate earlier in GSC-like cells compared with the other cell types. Three of these genomic windows are consistently earlier replicating in GSC-like cells compared with the other three cell types and are marked with an arrowhead. *Above* each bar is the fraction of the fourth chromosome that is earlier replicating in that cell type. (*H*) Comparison of replication timing between male cell types for the Y Chromosome shows the generally late replication timing of this chromosome. The fraction of the Y Chromosome that is earlier replicating in each cell type is presented *above* each bar. (*I*) Compared with female Kc cells, all male cells have a greater total genomic size of earlier replicating DNA on the X Chromosome. These early-replicating domains are located across the entirety of the X Chromosome. The fraction of the X Chromosome that is earlier replicating in each cell type is shown *above* each corresponding bar.

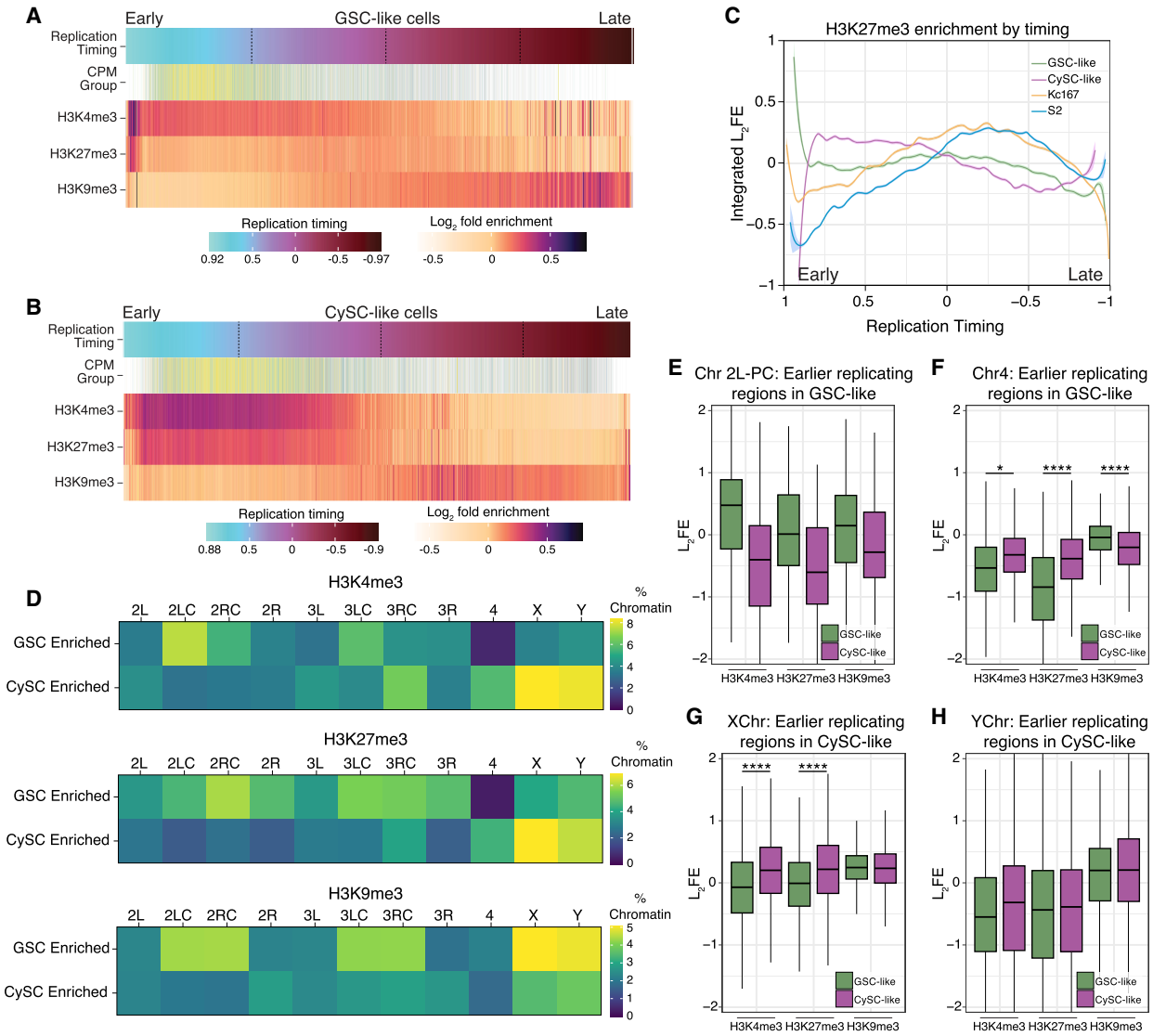

Figure 6. Cell-specific replication timing regimes correlate with cell-specific histone enrichment. (*A*) For GSC-like cells, the $\log_2$FE values for H3K4me3, H3K27me3, and H3K9me3 are shown for genomic locations ordered from early to late by their replication timing value. The expression level for genes (categorized and colored by their CPM group as in Fig. 3) is also shown, indicating genes with the highest expression are replicated earlier in S phase. (*B*) The $\log_2$FE values for H3K4me3, H3K27me3, and H3K9me3 are shown for CySC-like cells within genomic locations ordered by their replication timing (from early to late). Gene expression level (categorized and colored by CPM group) is also shown, indicating genes with the highest expression are replicated earlier in S phase. (*C*) The enrichment levels of H3K27me3 are plotted according to replication timing for the GSC-like, CySC-like, Kc167, and S2 cells, demonstrating increased H3K27me3 enrichment at regions that replicate early in CySC-like cells compared with the other three cell types. (*D*) Percentage of chromatin within in each indicated chromosomal domain was calculated and categorized as enriched in either GSC-like or CySC-like cells. Cell-specific enriched regions are considered as having $\log_2$FE values >0.2 in one cell type and <−0.2 in the other. (*E–H*) Box and whisker plots of $\log_2$FE for histone modifications in GSC-like (green) and CySC-like (magenta) cells on the indicated chromosomes. The values here are a subset of enrichment scores found in genomic regions that replicate earlier in the indicated cell type. (PC) Pericentromeric region, (*) statistical significance as measured by a paired sample *t*-test (Supplemental Table S5).

of which are cell-type specific (Rhind and Gilbert 2013). To investigate this relationship, we integrated our replication timing data with the cell-type-specific histone modification profiles generated in this study. Additionally, we reanalyzed published Repli-seq and ChIP-chip data from Kc167 and S2 cells to compare those in vitro data sets with our in vivo results (Kharchenko et al. 2011; Lubelsky et al. 2014).

Consistent with previous findings in Kc167 and S2 cells (Eaton et al. 2011), H3K4me3 is enriched at early-replicating regions, coinciding with genes that have the highest expression levels (Fig. 6A,B; Supplemental Fig. S7A–C). Accordingly, elevated H3K4me3 is present at the TSSs of genes located in the early-replicating fraction in both GSC-like and CySC-like cells (Supplemental Fig. S7E,F). In contrast, H3K9me3 is found in gene-poor and late-replicating regions across all cell types (Fig. 6A,B; Supplemental Fig. S7A,B,D–F).

On the other hand, H3K27me3 displays distinct enrichment patterns at different S-phase stages across cell types. In CySC-like cells, H3K27me3 is present throughout the early and early-mid S phase (Fig. 6B,C), overlapping with H3K4me3, and is enriched at

TSSs of genes replicating in these stages (Supplemental Fig. S7F). Notably, this H3K27me3 pattern is distinct from the other three cell types, further supporting the observation that there is a unique H3K27me3 chromatin signature in CySC-like cells. In contrast, H3K27me3 is predominantly enriched during mid S phase in GSC-like, Kc167, and S2 cells (Fig. 6A,C; Supplemental Fig. S7A,B). Consistently, in GSC-like cells, H3K27me3 is most enriched at TSSs of genes replicated during early-mid S phase (Supplemental Fig. S7E).

Our replication timing analysis revealed cell-type-specific timing regimes for pericentromeric heterochromatin on Chromosome 2L and globally for the fourth chromosome and the X and Y Chromosomes (Fig. 5). We next tested whether these regions have corresponding differences in chromatin landscapes. To compare histone modification differences across genomic regions between GSC-like and CySC-like cells, we defined a given locus as having cell-type-specific histone modification enrichment if its $\log_2$FE was >0.2 in one cell type and <−0.2 in the other. This analysis revealed strong overall correlations, suggesting broadly similar histone modification landscapes (Supplemental Fig. S7G). However, distinct GSC- or CySC-enriched histone modification regimes were also identified (Fig. 6D; Supplemental Fig. S7G, green and purple boxes). To quantify cell-type-specific chromatin features, we calculated the percentage of specific genomic regions enriched with each histone modification (Fig. 6D). For example, 7.4% of the pericentromeric region of Chromosome 2L in GSC-like cells is enriched for H3K4me3, compared with only 3.2% in CySC-like cells (Fig. 6D; Supplemental Table S7), aligning with its earlier replication timing in GSC-like cells (Fig. 5C). In contrast, the fourth chromosome in GSC-like cells shows almost no specific enrichment of H3K4me3 or H3K27me3 (Fig. 6D; Supplemental Table S7), despite its markedly early replication in this cell type. In CySC-like cells, a greater percentage of chromatin on the X and Y Chromosomes is enriched with both H3K4me3 and H3K27me3 (Fig. 6D).

We next evaluated histone modification enrichment scores at regions with distinct replication timing to assess correlations between cell-type-specific replication timing and chromatin features. In GSC-like cells, earlier replicating regions in Chromosome 2L pericentromeric heterochromatin displayed higher H3K4me3 enrichment compared with CySC-like cells (Fig. 6E; Supplemental Table S5). These earlier replicating regions on the fourth chromosome in GSC-like cells do not display a similar increase in H3K4me3 $\log_2$FE values compared with CySC-like cells (Fig. 6F; Supplemental Table S5), suggesting that the early replication of this chromosome may not be linked to a chromatin mark like H3K4me3.

In CySCs, the X and Y Chromosomes replicate earlier (Fig. 5C), and their earlier-replicating regions show higher levels of H3K4me3 and H3K27me3 compared with those in GSC-like cells (Fig. 6G,H; Supplemental Table S5). A similar observation was made for regions on the X and Y with earlier replication in GSC-like cells (Supplemental Fig. S7H,I, Supplemental Table S5), indicating a chromosome- and cell-type-specific relationship between replication timing and histone modifications. In summary, this integrative analysis reveals a relationship between cell-type- and chromosome-specific chromatin landscapes and DNA replication programs in *Drosophila* testis stem cells.

Selected features within differentially replicating regions in germline and somatic lineages

To explore the relationship between cell-type-specific replication timing and gene expression, we assessed gene-specific replication timing and expression differences between GSC-like and CySC-like cells within regions identified as differentially replicating. In the pericentromeric region of Chromosome 2L, several DEGs, such as *Marf1*, *mir-2490*, and *CR46253*, replicate earlier in GSC-like cells than in CySC-like cells (Fig. 7A,B). Although *Marf1* represses *nanos* expression and promotes meiotic progression during oogenesis in the female germline (Kawaguchi et al. 2020), the functions of *Marf1*, *mir-2490*, and *CR46253* in the male germline remain unknown. Notably, the genomic loci for these regulatory RNAs are associated with Orc2 binding sites, suggesting potential replication origins within this region (Fig. 7B). These observed differences in replication timing between GSC-like and CySC-like cells may reflect cell-type-specific origin usage that could arise from transcriptional differences within this region.

Extending beyond Chromosome 2L, the X Chromosome also exhibits distinct replication timing and histone modification enrichment in a cell-type-specific manner. In male cells, the X Chromosome generally replicates early, with CySC-like cells displaying higher H3K4me3 enrichment (Fig. 6D). The correlation between early-replicating regions and active histone modification enrichment further supports the connection between chromatin state and replication timing. Categorizing X-linked genes by cell-type-specific replication timing revealed a strong alignment between earlier replication and higher expression in the corresponding cell type (Fig. 7C,D). Notably, GSC-like cells showed more noncoding genes in early-replicating regions, suggesting a potential regulatory role for noncoding RNAs in this cell type (Fig. 7E,F).

Similarly, distinct replication patterns are also observed on the fourth chromosome. Several loci on the fourth chromosome replicate earlier in GSC-like cells across all pair-wise comparisons (Fig. 5G). One 64 kb domain contains six tandem genes that synchronously replicate early (Fig. 7G), clustering in the early GSC, late CySC quadrant (Fig. 7H). This region has five protein-coding genes and one uncharacterized lncRNA. This region is also associated with an Orc2 binding site, suggesting cell-type-specific origin usage (Fig. 7G).

The Y Chromosome also follows distinct replication timing patterns, with certain genes exhibiting early replication in a cell-type-specific manner despite its largely late-replicating nature. Functional data on the 16 annotated protein-coding genes on the Y Chromosome remains limited. For example, the *CCY* gene replicates early in CySC-like cells (Fig. 7I) and is essential for sperm individualization during late spermiogenesis, although its role in somatic gonadal cells remains unknown (Hafezi et al. 2020; Zhang et al. 2020). The presence of these genes in cell-type-specific early-replicating regions suggests their unexplored roles within the somatic lineage.

Taken together, these findings reveal links between replication timing, chromatin state, and cell identity. In summary, our replication timing data aligns with the cell-type-specific chromatin landscape, highlighting distinct regulatory regimes for the X and Y Chromosomes and the fourth chromosome in the soma versus germline. A broader pattern emerges: Regions that are typically heterochromatic in differentiated cells replicate earlier in GSC-like cells. This is reminiscent of findings in *Drosophila* female GSCs and cultured mouse embryonic stem cells, which also exhibit reduced heterochromatic marks compared to differentiated cells (Rausch et al. 2020; Pang et al. 2023). Thus, the male germline provides a valuable system to study gene expression, chromatin regulation, and DNA replication in endogenous adult stem-cell systems of a multicellular organism.

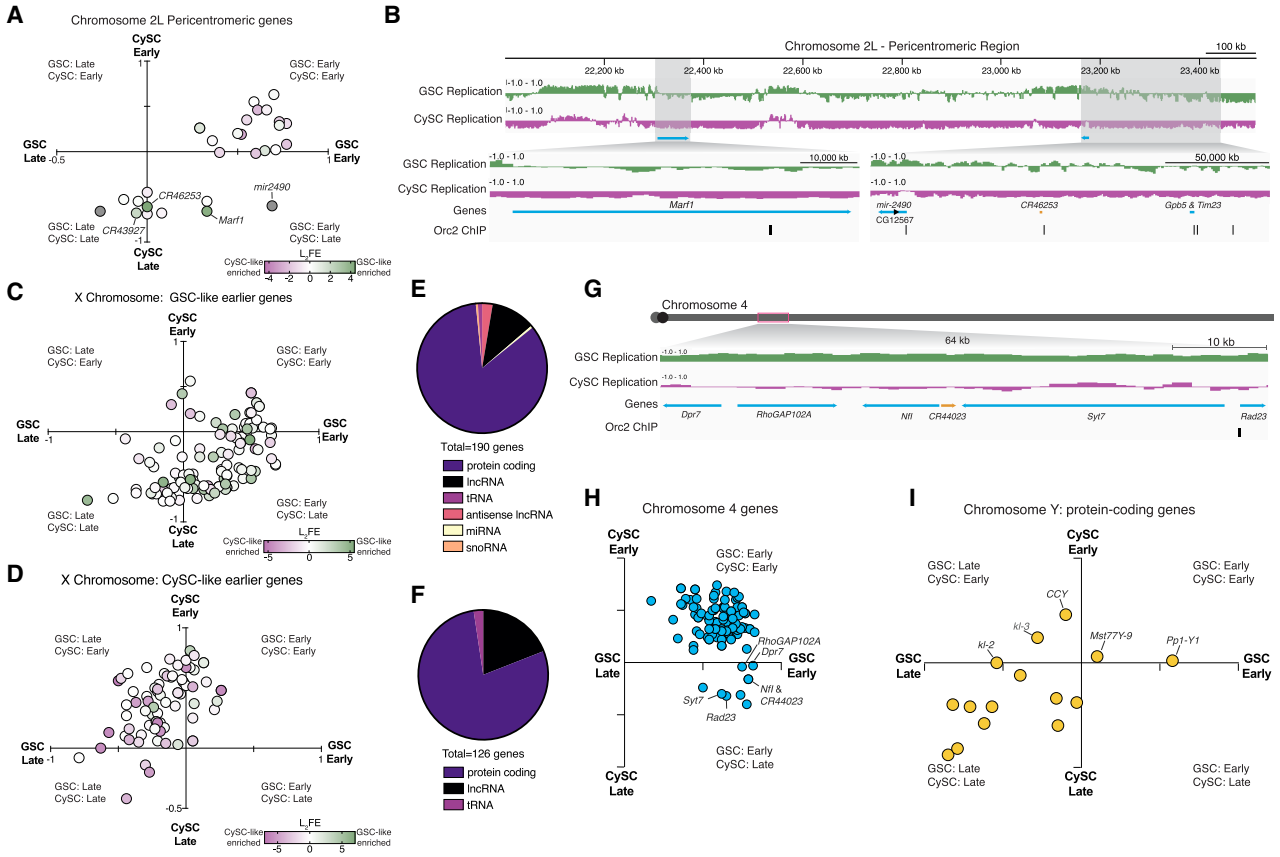

Figure 7. Selected genomic features within differentially replicating regions. (*A*) Scatterplot of the GSC-like (*x*-axis) and CySC-like (*y*-axis) replication timing values for genes located within the pericentromeric region of Chromosome 2L. Each data point represents a gene, in which each gene is colored by its $\log_2$FE value calculated by differential gene expression analysis of our scRNA-seq (Supplemental Table S2). Green represents transcript enrichment ($\log_2$FE) in GSC-like cells, whereas purple indicates enrichment in CySC-like cells. (*B*) A genome-browser image of the pericentromeric region of Chromosome 2L. In green are the replication timing tracks for GSC-like cells, in which the replication timing tracks for CySC-like cells are in magenta. Shown highlighted are the genes found to have differential replication timing and gene expression in GSC-like cells (blue arrows are protein-coding genes, and orange bars are noncoding RNAs). Also indicated is the location of Orc2 binding sites, which represent putative origins of replication. (*C*,*D*) Scatterplots of the GSC-like (*x*-axis) and CySC-like (*y*-axis) replication timing values for genes located on the X Chromosome, separated by whether they replicate earlier in GSC-like or CySC-like cells. Each data point represents a gene, in which each gene is colored by its $\log_2$FE value, which is calculated using differential gene expression analysis of the scRNA-seq (Supplemental Table S2). Green represents transcript enrichment in GSC-like cells, whereas purple indicates enrichment in CySC-like cells. (*E*,*F*) Shown is the proportion of gene types that replicate earlier in GSC-like or CySC-like cells. The majority are protein-coding genes, and the next largest gene category is long noncoding RNAs. (*G*) A genome-browser image of the fourth chromosome with one 64 kb region highlighted that is earlier replicating in GSC-like cells. The replication timing tracks for GSC-like cells are in green, and the replication timing tracks for CySC-like are magenta. Shown is the location of six tandem genes (protein coding in blue) residing in this earlier replicating domain, including a noncoding RNA (in orange) and Orc2 binding site. (*H*) Scatterplot of the GSC-like (*x*-axis) and CySC-like (*y*-axis) replication timing values for genes located on the fourth chromosome. Each data point represents a gene. Genes present within the 64 kb region cluster together as earlier replicating in GSC-like cells. (*I*) Scatterplot of the GSC-like (*x*-axis) and CySC-like (*y*-axis) replication timing values for genes located on the Y Chromosome. Each data point represents a gene. Genes that replicate earlier in CySC-like cells with potential roles in male fertility are indicated as marked.

Discussion

Understanding the mechanisms underlying cell fate specification and fate transitions is essential to developmental and stem-cell biology. In this study, we integrated transcriptional profiling, chromatin landscape analysis, and one of the first in vivo replication timing studies in adult stem cells to identify both shared and distinct regulatory mechanisms of *Drosophila* male germline and somatic cyst stem cells. We further compared our in vivo data sets with in vitro cultured *Drosophila* cell lines. In this way, we uncovered differences that were stem-cell-type specific in genomic and epigenomic features. To enable these studies, we used a stem-cell tumor model that provided sufficient material for multiomic profiling. Although our results were derived from this model, many of our findings align with known features of wild-type germline and cyst stem cells. This supports the model's utility as a platform for generating hypothesis and for guiding future investigations in wild-type tissue.

Our transcriptional profiling highlights a fundamental regulatory dichotomy between GSC-like and CySC-like cells. First, CySC-like cells rely on intercellular communication, with many highly expressed genes associated with signaling pathways that coordinate germline–soma interactions (Papagiannouli 2014; Vidaurre and Chen 2021). Second, GSC-like cells likely have a greater focus on regulating the chromatin landscape, with an overrepresentation of DNA replication and chromatin-modifying factors. This difference aligns with the well-established roles of intercellular signaling in coordinating GSC and CySC identity

and function. Although intercellular communication appears an essential function for the somatic lineage, the strong enrichment of chromatin factors in GSCs suggests that chromatin regulation plays a more dominant role in regulating GSC identity and activity.

Cell-type-specific heterochromatin replication timing

Our study reinforces the well-established relationship between chromatin features and replication timing, in which transcriptionally active euchromatic regions replicate early and transcriptionally inactive heterochromatic regions replicate late. However, by comparing these dynamics between two distinct adult stem-cell populations in vivo, we find differences that are stem-cell-type specific. Notably, we found that heterochromatic domains have locations that replicate earlier in GSC-like cells compared with CySC-like and cultured cells, suggesting fundamental differences in heterochromatin regulation between germline and somatic lineages.

A distinction between GSC-like and CySC-like cells is the abundance and broad distribution of H3K27me3, a facultative heterochromatin mark established by the Polycomb complex that is typically associated with gene silencing and cell identity maintenance (Wiles and Selker 2017). In CySC-like cells, H3K27me3 enrichment displays a canonical pattern, in which lower expressed genes exhibit higher levels of this mark. It is possible that the extensive presence of H3K27me3 in CySCs serves to restrict gene expression and reinforce the CC fate. This may reflect their unique division pattern; a single asymmetric cell division produces a self-renewed CySC daughter and a differentiating CC daughter. Two postmitotic CCs form a unit to support the differentiating germline for the duration of spermatogenesis, which takes ∼10 days at 25°C (Fabian and Brill 2012; Zoller and Schulz 2012). Therefore, the restriction of H3K27me3 could reinforce somatic CC identity, reflecting an early commitment to a terminal fate in this lineage.

In the female *Drosophila* germline lineage, constitutive pericentromeric heterochromatin formation begins in the germline cyst progeny of GSCs, whereas Polycomb-mediated gene repression suppresses male germline and somatic lineage genes (Pang et al. 2023). Further genomic and genetic studies in the female germline revealed an open chromatin environment in GSCs (DeLuca et al. 2020). In female GSCs, there is a noncanonical H3K27me3 distribution, whereby this modification is present in low amounts on active chromatin as well as on transcriptionally inactive loci (DeLuca et al. 2020). Here, we observe a similar trend in male GSCs, in which there is a roughly equivalent amount of H3K27me3 across all gene categories regardless of their expression levels, suggesting that low, non-gene-specific H3K27me3 may be an epigenetic feature of undifferentiated cells (DeLuca et al. 2020). However, in testes enriched with mitotic differentiating SG cells, the H3K27me3 pattern displays the canonical inverse correlation between enrichment and gene expression levels (Gan et al. 2010). As germ cells progress to meiotic spermatocytes, Polycomb function is counteracted, likely to allow derepression of sperm differentiation genes (Chen et al. 2005, 2011). Taken together, these findings indicate developmentally regulated Polycomb activity across distinct germ-cell stages in the *Drosophila* male germline.

Our finding that pericentromeric heterochromatin replicates early in GSCs aligns with published studies in mouse embryonic stem cells, which demonstrate that pericentromeric heterochromatin shifts from early to late replicating upon differentiation (Rausch et al. 2020). An additional key insight from that work was the significantly higher proportion of unidirectional replication forks in mouse embryonic stem cells (∼13%) compared with differentiated human cell lines (∼7%) (Rausch et al. 2020). Similarly, a notable 35% of replication forks are unidirectional in the *Drosophila* germline compared with ∼17% in somatic cells (Wooten et al. 2019; Davis et al. 2025). This trend of higher unidirectional fork usage in less differentiated states appears to be consistent across species.

In addition, activated origins in mouse embryonic stem cells are spaced at half the distance of that in somatic cells, indicating that stem cells activate twice as many origins of replication (Rausch et al. 2020). Although future studies in *Drosophila* GSCs are needed to determine whether the higher incidence of unidirectional replication forks corresponds to reduced interorigin distances, the elevated expression of DNA replication-related genes supports a model of increased replication demand in these cells. Furthermore, globally reduced H3K27me3 may create a permissive chromatin environment for increased unidirectional replication forks and origin activation. This supports the idea that unique replication dynamics may underlie specialized genome regulation in stem cells. These features may reflect developmental constraints on cell fate transitions or represent lineage-specific adaptations. Notably, our observation of early replication at the rDNA locus, which is well established to replicate unidirectionally (Gerber et al. 1997), supports this model.

In parallel with these replication features, the *Drosophila* germline exhibits a striking pattern of histone inheritance: Old histones, synthesized in the previous cell cycle, are preferentially incorporated onto the leading strand during DNA synthesis, whereas newly synthesized histones are biased toward the lagging strand (Wooten et al. 2019; Davis et al. 2025). This produces sister chromatids asymmetrically enriched with different histone populations, which are then differentially segregated such that old-histone-enriched sisters are retained in the self-renewing GSC, whereas the GB inherits new-histone-enriched sister chromatids (Tran et al. 2012; Ranjan et al. 2019). The elevated incidence of unidirectional forks may facilitate this global histone asymmetry, enabling extended tracts of old or new histone deposition. Early unidirectional replication at the rDNA locus may serve as a key organizing feature in establishing such genome-wide histone asymmetry in *Drosophila* GSCs. Together, these mechanisms may ensure the faithful inheritance of epigenetic information during stem-cell asymmetric cell division, by preserving stem-cell identity while allowing for flexible gene regulation in the differentiating progeny.

Recent studies in budding yeast suggest rDNA replication can influence anaphase onset, with extended rDNA repeats potentially delaying replication to prevent premature chromosome segregation (Kwan et al. 2023). In *Drosophila* germ cells, rDNA copy number decreases during aging yet can be restored in GSCs of young males in the following generation (Lu et al. 2018; Watase et al. 2022; Nelson et al. 2023). The mechanism underlying this generational recovery remains unknown. Early replication of the rDNA locus in GSC-like cells may present a strategy for maintaining or restoring rDNA copy number for subsequent generations, which might be less efficient if replication occurred later in the S phase. This preferential timing of rDNA replication in stem cells may therefore serve a critical function in long-term germline and organismal maintenance. Future studies can further clarify how this unique replication feature contributes to stem-cell genome integrity and lineage continuity.

Chromosome-specific replication timing profiles and regulatory roles for noncoding RNAs

Our work also uncovered chromosome-specific differences in histone modification enrichment and replication timing, particularly for the X Chromosome and the fourth chromosome. Historically, the fourth chromosome is considered as entirely heterochromatic, based on its high percentage of repetitive elements, lack of recombination, and high levels of HP1 and H3K9me2 (Haynes et al. 2007; Riddle et al. 2008). Previous studies in *Drosophila* suggest that the fourth chromosome largely shares chromatin features with pericentric heterochromatin, although it also contains some euchromatic regions (Haynes et al. 2007; Riddle et al. 2008). Unexpectedly, we found this chromosome replicates earlier in GSC-like cells than in CySC-like and other somatic cells. The biological significance of its early replication remains unclear. One possibility is that early replication of the fourth chromosome in GSC-like cells reflects a regulatory role for this chromosome that is specific to GSCs. Alternatively, this timing pattern may result from its similar chromatin composition to pericentromeric heterochromatin rather than from a regulatory process. Further studies are required to determine whether the early replication timing of the fourth chromosome in the male GSC-like cells has biological relevance for genome stability or gene regulation.

Our work also identified regulatory noncoding RNAs enriched in genomic regions undergoing coordinated changes in replication timing, chromatin state, and transcriptional activity, including those within the fourth chromosome and the pericentromeric heterochromatin of Chromosome 2. Although regulatory RNAs have historically been challenging to study, comparative analyses like ours allow for identifying them for further functional characterization. Previous studies have shown that ~30% of *Drosophila* testis-specific lncRNAs function during late spermiogenesis, regulating nuclear condensation, sperm individualization, and other terminal differentiation processes (Wen et al. 2016). However, their roles in early spermatogenesis, particularly in stem cells, remain poorly understood. Notably, several noncoding RNAs located in differentially replicating regions were also differentially expressed in GSC-like cells. It is possible that their transcription promotes an open chromatin environment, facilitating origin recognition and early replication. Rather than acting through their RNA products, these transcripts may instead provide a mechanism to achieve the elevated origin activation observed in stem cells. An intriguing possibility is that the inherent directionality of RNA transcription could influence coordinated replication origin activation and directionality of fork progression. By identifying candidate noncoding RNAs situated in regions with stem-cell-specific replication timing, our findings provide a foundation for investigating their functions in stem-cell maintenance, differentiation, and genome regulation.

Our findings reinforce our knowledge that the male X Chromosome maintains a unique chromatin environment that supports its well-established role in dosage compensation in somatic cells (Samata and Akhtar 2018). In CySC-like cells, the X Chromosome displays signatures of open chromatin consistent with this function, including H3K4me3 (this study), H4K16ac, and early replication (Rastelli and Kuroda 1998; Anderson et al. 2023). In GSC-like cells in which dosage compensation is inactive, the X Chromosome still replicates early. Previous studies in male and female *Drosophila* cell lines (Clone8 and Kc cells, respectively) similarly demonstrated that the X Chromosome replicates entirely during early S phase, even at genes enriched with H4K16ac that did not undergo gene dosage compensation (Schwaiger et al. 2009). Based on these findings, H4K16ac was proposed to associate more with early replication than with transcriptional activity. However, our data show that early replication persists in male GSCs even in the absence of this mark. Together, these results possibly suggest a connection between replication timing of the X Chromosome and chromatin accessibility, as opposed to replication timing being solely linked to transcriptional output or H4K16ac enrichment (Schwaiger et al. 2009). Our findings support a model that the X Chromosome's early replication timing in the male germline is maintained through dosage compensation-independent mechanisms, likely involving chromatin accessibility features.

In conclusion, by integrating transcriptional, chromatin, and replication timing analyses, our data provide a comprehensive framework for understanding the unique genomic regulation of male germline and somatic stem cells. Altogether, our findings reveal distinct fundamental divergence in regulatory mechanisms, including heterochromatin replication timing programs, chromosome-specific epigenetic differences, and potentially novel roles for lncRNAs in stem-cell genome organization. These findings provide new insights into stem-cell-specific genome regulation and establish a foundation for future studies on the epigenetic and replication dynamics of in vivo adult stem cells.

Methods

Fly husbandry

Fly stocks were maintained on standard molasses food (Bloomington recipe) at 25°C. A complete list of fly stocks and sources is provided in the Supplemental Materials. For genomic experiments, strains with switchable dual-tagged histone cassettes were introduced to a background containing a *UAS-upd* transgene (kindly provided by Dr. Stephen DiNardo, University of Pennsylvania) using standard fly genetics. Male progeny of the correct genotype were aged for ~2 days posteclosion before dissection and preparation for scRNA-seq, ChIC-ChIP-seq, or Repli-seq. For immunostaining experiments, young males (1–5 days old) were collected from fresh flips.

Immunostaining and image quantification

We used standard immunostaining approaches to perform both whole-mount and squash immunostaining of wild-type and *upd*-tumor testes. A detailed description of both approaches is included in the Supplemental Materials along with a complete list of all antibodies used in this study. For whole-mount staining, dissected testes were fixed, incubated with primary and secondary antibodies, counterstained with Hoechst, and imaged by confocal microscopy. For the squash method, *upd* tumor testes were ruptured, flash-frozen, ethanol-fixed, and stained with antibodies using similar incubation and wash steps prior to imaging. GFP-tagged Orc1, MCM2, and Caf1-105 fusion proteins were quantified from whole-mounted wild-type GSCs and CySCs using Imaris image analysis, with GFP intensity normalized to DNA content by Hoechst signal. Normalized GFP values were $\log_2$-transformed, plotted, and compared using a Mann–Whitney *U* test.

10x Genomics scRNA-seq

For scRNA-seq, tumor testes from *nanos* > Upd, H3-GFP or *tj* > Upd, H3-GFP flies were dissociated into single-cell suspensions using TrypLE Express and collagenase, followed by sequential filtration and washing to remove debris. Cell viability and counts were

assessed with trypan blue prior to library preparation. scRNA-seq libraries were generated using the 10x Genomics Chromium next GEM single-cell 3′ kit v3.1 according to the manufacturer's protocol, pooled to 4 nM, and sequenced using an Illumina NovaSeq S1 flow cell at the Johns Hopkins Genomics Core.

Cell-specific sequential chromatin immunocleavage–ChIP seq

Cell-specific sequential chromatin immunocleavage (ChIC)–ChIP was modified from an existing ChIC protocol optimized in the *upd* tumor (Chandrasekhara et al. 2023). In this study, ChIC-ChIP was performed to profile the H3K4me3, H3K27me3, and H3K9me3 histone modifications in *upd* tumor testes expressing H3-GFP in either GSC-like or CySC-like cells. In brief, *upd* tumor testes were dissociated into single-cell suspensions, cross-linked with formaldehyde, and lysed to release chromatin. Chromatin was incubated with a Protein A–MNase-antibody complex to direct cleavage in the cell type expressing H3-GFP. This was followed by controlled MNase digestion to release soluble fragments. Antibody-coupled magnetic beads were prepared in parallel and used to capture target chromatin, which underwent sequential low- and high-salt washes before elution. Cross-links were reversed; DNA was purified by a spin-column cleanup; and both input and immunoprecipitated fractions were quantified. Sequencing libraries were prepared using the NEBNext DNA Ultra II DNA library kit and sequenced on the Illumina NovaSeq platform.

Replication sequencing

Repli-seq was performed on *upd* tumor testes expressing H3-GFP in either GSC-like or CySC-like cells according to a published protocol (Marchal et al. 2018). Briefly, *upd* tumor testes were dissected, incubated with BrdU, and dissociated to isolate nuclei. GFP-positive nuclei were sorted by flow cytometry to separate S-phase populations into four fractions (early, early-mid, late-mid, late), providing temporal resolution of replication dynamics. DNA was then extracted from about 10,000 nuclei per fraction, fragmented by sonication, and prepared for sequencing using the NEBNext Ultra II DNA library prep kit. BrdU-labeled nascent DNA was enriched by sequential immunoprecipitation with an anti-BrdU antibody followed by a secondary antimouse IgG and then purified after Proteinase K digestion. The recovered DNA was quantified, PCR-amplified, and pooled for sequencing on the Illumina NovaSeq platform.

Bioinformatics

All genomic findings are identified based on alignment to FlyBase's *Drosophila melanogaster* genome (release 6.47) (Öztürk-Çolak et al. 2024). Supplemental steps that support particular analyses are the following: only analyzing uniquely mapped ChIC-seq data (MAPQ ≥ 20), applying epigenomic borders of the pericentromeric heterochromatin for chromosome region summaries (Filion et al. 2010), trimming rDNA-adjacent noncoding DNA from the rDNA auxiliary sequence file (to summarize or plot the rDNA repeat unit), and regressing ChIC-ChIP enrichment on the unique transposon sequence set.

scRNA-seq analysis

To test the hypothesis that the GSC-like and CySC-like tumor cell populations are largely homogenous, we aligned and quantified the scRNA-seq UMI data using Cell Ranger (v7.0.0) with default parameters (Zheng et al. 2017). Our dimension reduction (UMAP) and clustering are derived from Seurat's SCTransform integrated assay (Butler et al. 2018; Hafemeister and Satija 2019). For quantification, single-cell data are denoised using DecontX for UMI quantification correction (Yang et al. 2020). The log-normalized gene expression is computed from the DecontX-corrected count for the gene, with a shifted logarithm (Ahlmann-Eltze and Huber 2023). Pseudobulk $\log_{10}$ CPM is computed, after a compatible isoform selection, reapplication of DecontX, and log transformation, using a linear model (Ritchie et al. 2015). Posterior log fold change estimates further enrich the downstream gene set enrichment, compared with pseudobulk log-scaled differences, by fitting a Bayesian regression coefficient estimate (Zhu et al. 2019). Our covariates are DecontX's contamination score, crossed with cell type. DEGs for GSC-like or CySC-like enrichment were selected by a *s*-value less than 10^{-4} and a log effect size (L_2FC) of at least 1.5, yielding enriched GO terms (Thomas et al. 2022).

ChIC-ChIP sequencing analysis

ChIC-seq reveals nucleosome occupancy, H3K4me3 enrichment, H3K27me3 enrichment, and H3K9me3 enrichment, in the bulk GSC-like and CySC-like cell genomic DNA libraries. Our ChIC-seq analyses produces sharp nucleosome positioning estimates as regression effects (intercept of H3 abundance and L_2FC of ChIC-ChIP treatment; 20 bp step) in which the model applied is maximum-likelihood negative binomial regression (Ahlmann-Eltze and Huber 2021). Positioning is made to be precise by filtering the paired-end fragment length and only binning the midpoint between the reads into the sliding genomic window. Monosomes are visible as local maxima in a genomic track, producing the finished ChIC-seq tracks, after estimating feature density from regression predictions: smoothing using a Gaussian kernel with sigma = 40 bp (Boyle et al. 2008). The log-fold enrichment of the IP "F-Seq" (Gaussian) track, relative to the H3 input track, reveals antibody binding to the monosome, with appropriate (20 bp) resolution to reveal the monosome midpoint location.

Repli-seq analysis

Repli-seq identifies genomic loci that are enriched in a certain interval of the S phase (in which the interval of the S phase is marked by molecular mass of DNA). Like our ChIC-seq regression, we bin the midpoints of Repli-seq single-end 100 bp reads or the properly paired alignment (up to 500 bp wide) into nonoverlapping 1 kb steps across the genome. We found that consecutive bins of fragments were statistically independent enough (in autocorrelation) to serve as a set of observations for regression. In a 3 kb window, we used the observations of three bins of DNA in either six or eight samples to infer a Bayesian logistic regression parameter (logit timing score), characterized by its posterior expected value. The timing parameter posterior distributions are compared to reject the null hypothesis of a static replication regime. Testing a coefficient to explain biological count data can be carried out via a likelihood ratio test (Love et al. 2014). We apply numerical integration to the full and reduced model likelihoods, summarized as a Bayes factor. For pairwise cell-type comparisons, the null hypothesis is rejected using the Bayes factor in regions of width at least 20 kb. Finally, for viewing and for marking early- and late-replicating chromatin, Repli-seq timing estimates can be smoothed using LOESS.

This version of the genomic tracks permits *Z*-scoring several cell types at every genomic location. Mean *Z*-scores across the chromosomal regions allow us to describe regions as having overall static choreography or replication bias.

Data access

All raw and processed sequencing data generated in this study have been submitted to the NCBI Gene Expression Omnibus (GEO;

https://www.ncbi.nlm.nih.gov/geo/) under accession number GSE291929. The genomics analysis scripts are available at GitHub (https://github.com/ringw/Upd-Germline-Genomics) and as Supplemental Code.

Competing interest statement

The authors declare no competing interests.

Acknowledgments

We thank Dr. Winston Timp and Siqi (Alice) Chen for technical support in performing the 10x Genomics scRNA-seq, Dr. Hao Zhang (Flow Cytometry and Cell Sorting Core Facility, Johns Hopkins Bloomberg School of Public Health) for assistance with Repli-seq cell sorting, and Hanhvy Bui (John Hopkins Integrated Imaging Center) for her initial efforts in developing a cell sorting protocol. We thank the Johns Hopkins Genetics Resources Core Facility for consultation and high-throughput sequencing. We also thank several members of Dr. Keji Zhao's group—Drs. Lixia Pan, Wai Lim Ku, Guangzhe Ge, Kairong Cui, Qingsong Tang, and Meiyuan Ji—for help in establishing the ChIC-seq protocol, sequencing submission, and data storage. Funding was provided by National Institutes of Health (NIH) Intramural funding (K.Z.); NIH R35 GM127075-01S1, American Cancer Society PF-19-131-01-DMC, and NIH MOSAIC K99GM145973 (J.A.U.); and NIH R35 GM127075, R01 HD102474, and the Howard Hughes Medical Institute (X.C.).

Author contributions: The project was conceptualized by J.A.U. and X.C. Validation of the *upd* tumor system was completed by R.G. and W.X., and all other experimentation was performed by J.A.U. The bioinformatic analysis was performed by D.R. and J.M.U. This manuscript was written and edited by J.A.U. and X.C. Support for experimentation and funding for this study was provided by J.A.U., K.Z., and X.C.

References

Ahlmann-Eltze C, Huber W. 2021. glmGamPoi: fitting Gamma-Poisson generalized linear models on single cell count data. *Bioinformatics* **36:** 5701–5702. doi:10.1093/bioinformatics/btaa1009

Ahlmann-Eltze C, Huber W. 2023. Comparison of transformations for single-cell RNA-seq data. *Nat Methods* **20:** 665–672. doi:10.1038/s41592-023-01814-1

Amoyel M, Bach EA. 2012. Functions of the *Drosophila* JAK-STAT pathway: lessons from stem cells. *JAKSTAT* **1:** 176–183. doi:10.4161/jkst.21621

Anderson JT, Henikoff S, Ahmad K. 2023. Chromosome-specific maturation of the epigenome in the *Drosophila* male germline. *eLife* **12:** RP89373. doi:10.7554/eLife.89373

Armstrong RL, Penke TJR, Strahl BD, Matera AG, McKay DJ, MacAlpine DM, Duronio RJ. 2018. Chromatin conformation and transcriptional activity are permissive regulators of DNA replication initiation in *Drosophila*. *Genome Res* **28:** 1688–1700. doi:10.1101/gr.239913.118

Boyle AP, Guinney J, Crawford GE, Furey TS. 2008. F-seq: a feature density estimator for high-throughput sequence tags. *Bioinformatics* **24:** 2537–2538. doi:10.1093/bioinformatics/btn480

Butler A, Hoffman P, Smibert P, Papalexi E, Satija R. 2018. Integrating single-cell transcriptomic data across different conditions, technologies, and species. *Nat Biotechnol* **36:** 411–420. doi:10.1038/nbt.4096

Chandrasekhara C, Ranjan R, Urban JA, Davis BEM, Ku WL, Snedeker J, Zhao K, Chen X. 2023. A single N-terminal amino acid determines the distinct roles of histones H3 and H3.3 in the *Drosophila* male germline stem cell lineage. *PLoS Biol* **21:** e3002098. doi:10.1371/journal.pbio.3002098

Chen X, Hiller M, Sancak Y, Fuller MT. 2005. Tissue-specific TAFs counteract polycomb to turn on terminal differentiation. *Science* **310:** 869–872. doi:10.1126/science.1118101

Chen X, Lu C, Prado JRM, Eun SH, Fuller MT. 2011. Sequential changes at differentiation gene promoters as they become active in a stem cell lineage. *Development* **138:** 2441–2450. doi:10.1242/dev.056572

Cheng J, Tiyaboonchai A, Yamashita YM, Hunt AJ. 2011. Asymmetric division of cyst stem cells in *Drosophila* testis is ensured by anaphase spindle repositioning. *Development* **138:** 831–837. doi:10.1242/dev.057901

Cherbas L, Gong L. 2014. Cell lines. *Methods* **68:** 74–81. doi:10.1016/j.ymeth.2014.01.006

Chereji RV, Ramachandran S, Bryson TD, Henikoff S. 2018. Precise genome-wide mapping of single nucleosomes and linkers in vivo. *Genome Biol* **19:** 19. doi:10.1186/s13059-018-1398-0

Das S, Caballero M, Kolesnikova T, Zhimulev I, Koren A, Nordman J. 2021. Replication timing analysis in polyploid cells reveals Rif1 uses multiple mechanisms to promote underreplication in Drosophila. *Genetics* **219:** iyab147. doi:10.1093/genetics/iyab147

Davis BEM, Snedeker J, Ranjan R, Wooten M, Barton SS, Blundon J, Chen X. 2025. Increased levels of lagging strand polymerase α in an adult stem cell lineage affect replication-coupled histone incorporation. *Sci Adv* **11:** 6799. doi:10.1126/sciadv.adu6799

DeLuca SZ, Ghildiyal M, Pang LY, Spradling AC. 2020. Differentiating *Drosophila* female germ cells initiate Polycomb silencing by regulating PRC2-interacting proteins. *eLife* **9:** e56922. doi:10.7554/eLife.56922

Eaton ML, Prinz JA, MacAlpine HK, Tretyakov G, Kharchenko PV, MacAlpine DM. 2011. Chromatin signatures of the *Drosophila* replication program. *Genome Res* **21:** 164–174. doi:10.1101/gr.116038.110

Eun SH, Shi Z, Cui K, Zhao K, Chen X. 2014. A non-cell-autonomous role of E(z) to prevent germ cells from turning on a somatic cell marker. *Science* **343:** 1513–1516. doi:10.1126/science.1246514

Eun SH, Feng L, Cedeno-Rosario L, Gan Q, Wei G, Cui K, Zhao K, Chen X. 2017. Polycomb group gene E(z) is required for spermatogonial dedifferentiation in *Drosophila* adult testis. *J Mol Biol* **429:** 2030–2041. doi:10.1016/j.jmb.2017.04.012

Fabian L, Brill JA. 2012. *Drosophila* spermiogenesis: big things come from little packages. *Spermatogenesis* **2:** 197–212. doi:10.4161/spmg.21798

Fabrizio JJ, Boyle M, DiNardo S. 2003. A somatic role for *eyes absent (eya)* and *sine oculis (so)* in *Drosophila* spermatocyte development. *Dev Biol* **258:** 117–128. doi:10.1016/S0012-1606(03)00127-1

Filion GJ, van Bemmel JG, Braunschweig U, Talhout W, Kind J, Ward LD, Brugman W, de Castro IJ, Kerkhoven RM, Bussemaker HJ, et al. 2010. Systematic protein location mapping reveals five principal chromatin types in *Drosophila* cells. *Cell* **143:** 212–224. doi:10.1016/j.cell.2010.09.009

Formosa T, Winston F. 2020. The role of FACT in managing chromatin: disruption, assembly, or repair? *Nucleic Acids Res* **48:** 11929–11941. doi:10.1093/nar/gkaa912

Fuller MT, Spradling AC. 2007. Male and female *Drosophila* germline stem cells: two versions of immortality. *Science* **316:** 402–404. doi:10.1126/science.1140861

Gan Q, Schones DE, Ho Eun S, Wei G, Cui K, Zhao K, Chen X. 2010. Monovalent and unpoised status of most genes in undifferentiated cell-enriched *Drosophila* testis. *Genome Biol* **11:** R42. doi:10.1186/gb-2010-11-4-r42

Gerber JK, Gögel E, Berger C, Wallisch M, Müller F, Grummt I, Grumm F. 1997. Termination of mammalian rDNA replication: polar arrest of replication fork movement by transcription termination factor TTF-I. *Cell* **90:** 559–567. doi:10.1016/S0092-8674(00)80515-2

Gönczy P, DiNardo S. 1996. The germ line regulates somatic cyst cell proliferation and fate during *Drosophila* spermatogenesis. *Development* **122:** 2437–2447. doi:10.1242/dev.122.8.2437

Hafemeister C, Satija R. 2019. Normalization and variance stabilization of single-cell RNA-seq data using regularized negative binomial regression. *Genome Biol* **20:** 296. doi:10.1186/s13059-019-1874-1

Hafezi Y, Sruba SR, Tarrash SR, Wolfner MF, Clark AG. 2020. Dissecting fertility functions of *Drosophila Y* chromosome genes with CRISPR. *Genetics* **214:** 977–990. doi:10.1534/genetics.120.302672

Haynes KA, Gracheva E, Elgin SCR. 2007. A distinct type of heterochromatin within *Drosophila melanogaster* chromosome 4. *Genetics* **175:** 1539–1542. doi:10.1534/genetics.106.066407

Hiller MA, Lin TY, Wood C, Fuller MT. 2001. Developmental regulation of transcription by a tissue-specific TAF homolog. *Genes Dev* **15:** 1021–1030. doi:10.1101/gad.869101

Hu X, Li M, Hao X, Lu Y, Zhang L, Wu G. 2021. The Osa-containing SWI/SNF chromatin-remodeling complex is required in the germline differentiation niche for germline stem cell progeny differentiation. *Genes (Basel)* **12:** 363. doi:10.3390/genes12030363

Hudson AG, Parrott BB, Qian Y, Schulz C. 2013. A temporal signature of epidermal growth factor signaling regulates the differentiation of germline cells in testes of *Drosophila melanogaster*. *PLoS One* **8:** e70678. doi:10.1371/journal.pone.0070678

Kawaguchi S, Ueki M, Kai T. 2020. *Drosophila* MARF1 ensures proper oocyte maturation by regulating nanos expression. *PLoS One* **15:** e0231114. doi:10.1371/journal.pone.0231114

Kawase E, Wong MD, Ding BC, Xie T. 2004. Gbb/Bmp signaling is essential for maintaining germline stem cells and for repressing *bam*

transcription in the *Drosophila* testis. *Development* **131:** 1365–1375. doi:10.1242/dev.01025
Kelly KK, Meadows SM, Cripps RM. 2002. *Drosophila* MEF2 is a direct regulator of Actin57B transcription in cardiac, skeletal, and visceral muscle lineages. *Mech Dev* **110:** 39–50. doi:10.1016/S0925-4773(01)00586-X
Kharchenko PV, Alekseyenko AA, Schwartz YB, Minoda A, Riddle NC, Ernst J, Sabo PJ, Larschan E, Gorchakov AA, Gu T, et al. 2011. Comprehensive analysis of the chromatin landscape in *Drosophila melanogaster*. *Nature* **471:** 480–485. doi:10.1038/nature09725
Kiger AA, White-Cooper H, Fuller MT. 2000. Somatic support cells restrict germline stem cell self-renewal and promote differentiation. *Nature* **407:** 750–754. doi:10.1038/35037606
Kiger AA, Jones DL, Schulz C, Rogers MB, Fuller MT. 2001. Stem cell self-renewal specified by JAK-STAT activation in response to a support cell cue. *Science* **294:** 2542–2545. doi:10.1126/science.1066707
Kouzarides T. 2007. Chromatin modifications and their function. *Cell* **128:** 693–705. doi:10.1016/j.cell.2007.02.005
Kuhn R, Kuhn C, Börsch D, Glätzer KH, Schäfer U, Schäfer M. 1991. A cluster of four genes selectively expressed in the male germ line of *Drosophila melanogaster*. *Mech Dev* **35:** 143–151. doi:10.1016/0925-4773(91)90064-D
Kwan EX, Alvino GM, Lynch KL, Levan PF, Amemiya HM, Wang XS, Johnson SA, Sanchez JC, Miller MA, Croy M, et al. 2023. Ribosomal DNA replication time coordinates completion of genome replication and anaphase in yeast. *Cell Rep* **42:** 112161. doi:10.1016/j.celrep.2023.112161
Leatherman JL, DiNardo S. 2008. *Zfh-1* controls somatic stem cell self-renewal in the *Drosophila* testis and nonautonomously influences germline stem cell self-renewal. *Cell Stem Cell* **3:** 44–54. doi:10.1016/j.stem.2008.05.001
Leatherman JL, DiNardo S. 2010. Germline self-renewal requires cyst stem cells and *stat* regulates niche adhesion in *Drosophila* testes. *Nat Cell Biol* **12:** 806–811. doi:10.1038/ncb2086
Li H, Janssens J, de Waegeneer M, Kolluru SS, Davie K, Gardeux V, Saelens W, David FPA, Brbić M, Spanier K, et al. 2022. Fly cell atlas: a single-nucleus transcriptomic atlas of the adult fruit fly. *Science* **375:** eabk2432. doi:10.1126/science.abk2432
Lin H, Yue L, Spradling AC. 1994. The *Drosophila* fusome, a germline-specific organelle, contains membrane skeletal proteins and functions in cyst formation. *Development* **120:** 947–956. doi:10.1242/dev.120.4.947
Love MI, Huber W, Anders S. 2014. Moderated estimation of fold change and dispersion for RNA-seq data with DESeq2. *Genome Biol* **15:** 550. doi:10.1186/s13059-014-0550-8
Lu KL, Nelson JO, Watase GJ, Warsinger-Pepe N, Yamashita YM. 2018. Transgenerational dynamics of rDNA copy number in *Drosophila* male germline stem cells. *eLife* **7:** e32421. doi:10.7554/eLife.32421
Lubelsky Y, Prinz JA, DeNapoli L, Li Y, Belsky JA, MacAlpine DM. 2014. DNA replication and transcription programs respond to the same chromatin cues. *Genome Res* **24:** 1102–1114. doi:10.1101/gr.160010.113
Marchal C, Sasaki T, Vera D, Wilson K, Sima J, Rivera-Mulia JC, Trevilla-García C, Nogues C, Nafie E, Gilbert DM. 2018. Genome-wide analysis of replication timing by next-generation sequencing with E/L Repliseq. *Nat Protoc* **13:** 819–839. doi:10.1038/nprot.2017.148
Matunis EL, Stine RR, de Cuevas M. 2012. Recent advances in *Drosophila* male germline stem cell biology. *Spermatogenesis* **2:** 137–144. doi:10.4161/spmg.21763
McKearin DM, Spradling AC. 1990. *bag-of-marbles*: a *Drosophila* gene required to initiate both male and female gametogenesis. *Genes Dev* **4:** 2242–2251. doi:10.1101/gad.4.12b.2242
Meiklejohn CD, Landeen EL, Cook JM, Kingan SB, Presgraves DC. 2011. Sex chromosome-specific regulation in the *Drosophila* male germline but little evidence for chromosomal dosage compensation or meiotic inactivation. *PLoS Biol* **9:** e1001126. doi:10.1371/journal.pbio.1001126
Nakatani T, Schauer T, Altamirano-Pacheco L, Klein KN, Ettinger A, Pal M, Gilbert DM, Torres-Padilla ME. 2023. Emergence of replication timing during early mammalian development. *Nature* **625:** 401–409. doi:10.1038/s41586-023-06872-1
Nelson JO, Slicko A, Yamashita YM. 2023. The retrotransposon R2 maintains *Drosophila* ribosomal DNA repeats. *Proc Natl Acad Sci* **120:** e2221613120. doi:10.1073/pnas.2221613120
Ng CL, Qian Y, Schulz C. 2019. Notch and delta are required for survival of the germline stem cell lineage in testes of *Drosophila melanogaster*. *PLoS One* **14:** e0222471. doi:10.1371/journal.pone.0222471
Öztürk-Çolak A, Marygold SJ, Antonazzo G, Attrill H, Goutte-Gattat D, Jenkins VK, Matthews BB, Millburn G, dos Santos G, Tabone CJ, et al. 2024. FlyBase: updates to the *Drosophila* genes and genomes database. *Genetics* **227:** iyad211. doi:10.1093/genetics/iyad211
Pang LY, De Luca S, Zhu H, Urban JM, Spradling AC. 2023. Chromatin and gene expression changes during female *Drosophila* germline stem cell development illuminate the biology of highly potent stem cells. *eLife* **12:** RP90509. doi:10.7554/eLife.90509
Papagiannouli F. 2014. Male stem cell niche and spermatogenesis in the *Drosophila* testis: a tale of germline-soma communication. In *Adult stem cell niches* (ed. Wislet-Gendebien S). IntechOpen, London. doi:10.5772/58756. https://www.intechopen.com/chapters/47159 (accessed April 8, 2025).
Parrott BB, Hudson A, Brady R, Schulz C. 2012. Control of germline stem cell division frequency: a novel, developmentally regulated role for epidermal growth factor signaling. *PLoS One* **7:** e36460. doi:10.1371/journal.pone.0036460
Pratto F, Brick K, Cheng G, Lam KWG, Cloutier JM, Dahiya D, Wellard SR, Jordan PW, Camerini-Otero RD. 2021. Meiotic recombination mirrors patterns of germline replication in mice and humans. *Cell* **184:** 4251–4267.e20. doi:10.1016/j.cell.2021.06.025
Ranjan R, Snedeker J, Chen X. 2019. Asymmetric centromeres differentially coordinate with mitotic machinery to ensure biased sister chromatid segregation in germline stem cells. *Cell Stem Cell* **25:** 666–681.e5. doi:10.1016/j.stem.2019.08.014
Rastelli L, Kuroda MI. 1998. An analysis of maleless and histone H4 acetylation in *Drosophila melanogaster* spermatogenesis. *Mech Dev* **71:** 107–117. doi:10.1016/S0925-4773(98)00009-4
Rausch C, Weber P, Prorok P, Hörl D, Maiser A, Lehmkuhl A, Chagin VO, Casas-Delucchi CS, Leonhardt H, Cristina Cardoso M. 2020. Developmental differences in genome replication program and origin activation. *Nucleic Acids Res* **48:** 12751–12777. doi:10.1093/nar/gkaa1124
Raz AA, Vida GS, Stern SR, Mahadevaraju S, Fingerhut JM, Viveiros JM, Pal S, Grey JR, Grace MR, Berry CW, et al. 2023. Emergent dynamics of adult stem cell lineages from single nucleus and single cell RNA-seq of *Drosophila* testes. *eLife* **12:** e82201. doi:10.7554/eLife.82201
Rhind N, Gilbert DM. 2013. DNA replication timing. *Cold Spring Harb Perspect Biol* **5:** a010132. doi:10.1101/cshperspect.a010132
Riddle NC, Leung W, Haynes KA, Granok H, Wuller J, Elgin SCR. 2008. An investigation of heterochromatin domains on the fourth chromosome of *Drosophila melanogaster*. *Genetics* **178:** 1177–1191. doi:10.1534/genetics.107.081828
Ritchie ME, Phipson B, Wu D, Hu Y, Law CW, Shi W, Smyth GK. 2015. *limma* powers differential expression analyses for RNA-sequencing and microarray studies. *Nucleic Acids Res* **43:** e47. doi:10.1093/nar/gkv007
Samata M, Akhtar A. 2018. Dosage compensation of the X chromosome: a complex epigenetic assignment involving chromatin regulators and long noncoding RNAs. *Annu Rev Biochem* **87:** 323–350. doi:10.1146/annurev-biochem-062917-011816
Schulz C, Wood CG, Jones DL, Tazuke SI, Fuller MT. 2002. Signaling from germ cells mediated by the *rhomboid* homolog *stet* organizes encapsulation by somatic support cells. *Development* **129:** 4523–4534. doi:10.1242/dev.129.19.4523
Schwaiger M, Stadler MB, Bell O, Kohler H, Oakeley EJ, Sehübeler D. 2009. Chromatin state marks cell-type- and gender-specific replication of the *Drosophila* genome. *Genes Dev* **23:** 589–601. doi:10.1101/gad.511809
Shevelyov YY, Ulianov SV, Gelfand MS, Belyakin SN, Razin SV. 2022. Dosage compensation in *Drosophila*: its canonical and non-canonical mechanisms. *Int J Mol Sci* **23:** 10976. doi:10.3390/ijms231810976
Shi Z, Lim C, Tran V, Cui K, Zhao K, Chen X. 2020. Single-cyst transcriptome analysis of *Drosophila* male germline stem cell lineage. *Development* **147:** dev184259. doi:10.1242/dev.184259
Shivdasani AA, Ingham PW. 2003. Regulation of stem cell maintenance and transit amplifying cell proliferation by TFG-beta signaling in *Drosophila* spermatogenesis. *Curr Biol* **13:** 2065–2072. doi:10.1016/j.cub.2003.10.063
Siefert JC, Georgescu C, Wren JD, Koren A, Sansam CL. 2017. DNA replication timing during development anticipates transcriptional programs and parallels enhancer activation. *Genome Res* **27:** 1406–1416. doi:10.1101/gr.218602.116
Takahashi S, Kyogoku H, Hayakawa T, Miura H, Oji A, Kondo Y, Takebayashi S, Kitajima T, Hiratani I. 2024. Embryonic genome instability upon DNA replication timing program emergence. *Nature* **633:** 686–694. doi:10.1038/s41586-024-07841-y
Thomas PD, Ebert D, Muruganujan A, Mushayahama T, Albou LP, Mi H. 2022. PANTHER: making genome-scale phylogenetics accessible to all. *Protein Sci* **31:** 8–22. doi:10.1002/pro.4218
Tran V, Lim C, Xie J, Chen X. 2012. Asymmetric division of *Drosophila* male germline stem cell shows asymmetric histone distribution. *Science* **338:** 679–682. doi:10.1126/science.1226028
Tulina N, Matunis E. 2001. Control of stem cell self-renewal in *Drosophila* spermatogenesis by JAK-STAT signaling. *Science* **294:** 2546–2549. doi:10.1126/science.1066700
Tyagi M, Imam N, Verma K, Patel AK. 2016. Chromatin remodelers: We are the drivers!! *Nucleus* **7:** 388–404. doi:10.1080/19491034.2016.1211217
Urban J, Kuzu G, Bowman S, Scruggs B, Henriques T, Kingston R, Adelman K, Tolstorukov M, Larschan E. 2017. Enhanced chromatin accessibility

of the dosage compensated *Drosophila* male X-chromosome requires the CLAMP zinc finger protein. *PLoS One* **12:** e0186855. doi:10.1371/journal.pone.0186855

Vedelek V, Bodai L, Grézal G, Kovács B, Boros IM, Laurinyecz B, Sinka R. 2018. Analysis of *Drosophila melanogaster* testis transcriptome. *BMC Genomics* **19:** 697. doi:10.1186/s12864-018-5085-z

Vidaurre V, Chen X. 2021. Epigenetic regulation of *Drosophila* germline stem cell maintenance and differentiation. *Dev Biol* **473:** 105–118. doi:10.1016/j.ydbio.2021.02.003

Watase GJ, Nelson JO, Yamashita YM. 2022. Nonrandom sister chromatid segregation mediates rDNA copy number maintenance in *Drosophila*. *Sci Adv* **8:** 4443. doi:10.1126/sciadv.abo4443

Wen K, Yang L, Xiong T, Di C, Ma D, Wu M, Xue Z, Zhang X, Long L, Zhang W, et al. 2016. Critical roles of long noncoding RNAs in *Drosophila* spermatogenesis. *Genome Res* **26:** 1233–1244. doi:10.1101/gr.199547.115

Wiles ET, Selker EU. 2017. H3k27 methylation: a promiscuous repressive chromatin mark. *Curr Opin Genet Dev* **43:** 31–37. doi:10.1016/j.gde.2016.11.001

Williams RW, Rubin GM. 2002. *ARGONAUTE1* is required for efficient RNA interference in *Drosophila* embryos. *Proc Natl Acad Sci* **99:** 6889–6894. doi:10.1073/pnas.072190799

Witt E, Benjamin S, Svetec N, Zhao L. 2019. Testis single-cell RNA-seq reveals the dynamics of de novo gene transcription and germline mutational bias in *Drosophila*. *eLife* **8:** e47138. doi:10.7554/eLife.47138

Wooten M, Snedeker J, Nizami ZF, Yang X, Ranjan R, Urban E, Kim JM, Gall J, Xiao J, Chen X. 2019. Asymmetric histone inheritance via strand-specific incorporation and biased replication fork movement. *Nat Struct Mol Biol* **26:** 732–743. doi:10.1038/s41594-019-0269-z

Yang S, Corbett SE, Koga Y, Wang Z, Johnson WE, Yajima M, Campbell JD. 2020. Decontamination of ambient RNA in single-cell RNA-seq with DecontX. *Genome Biol* **21:** 57. doi:10.1186/s13059-020-1950-6

Young MD, Willson TA, Wakefield MJ, Trounson E, Hilton DJ, Blewitt ME, Oshlack A, Majewski IJ. 2011. ChIP-seq analysis reveals distinct H3K27me3 profiles that correlate with transcriptional activity. *Nucleic Acids Res* **39:** 7415–7427. doi:10.1093/nar/gkr416

Yu J, Li Z, Fu Y, Sun F, Chen X, Huang Q, He L, Yu H, Ji L, Cheng X, et al. 2023. Single-cell RNA-sequencing reveals the transcriptional landscape of ND-42 mediated spermatid elongation via mitochondrial derivative maintenance in *Drosophila* testes. *Redox Biol* **62:** 102671. doi:10.1016/j.redox.2023.102671

Zhang J, Luo J, Chen J, Dai J, Montell C. 2020. The role of Y chromosome genes in male fertility in *Drosophila melanogaster*. *Genetics* **215:** 623–633. doi:10.1534/genetics.120.303324

Zhang Y, Huang Y, Dong Y, Liu X, Kou X, Zhao Y, Zhao A, Sun J, Su Z, Li Z, et al. 2021. Unique patterns of H3K4me3 and H3K27me3 in 2-cell-like embryonic stem cells. *Stem Cell Reports* **16:** 458–469. doi:10.1016/j.stemcr.2021.01.020

Zheng GXY, Terry JM, Belgrader P, Ryvkin P, Bent ZW, Wilson R, Ziraldo SB, Wheeler TD, McDermott GP, Zhu J, et al. 2017. Massively parallel digital transcriptional profiling of single cells. *Nat Commun* **8:** 14049. doi:10.1038/ncomms14049

Zhu A, Ibrahim JG, Love MI. 2019. Heavy-tailed prior distributions for sequence count data: removing the noise and preserving large differences. *Bioinformatics* **35:** 2084–2092. doi:10.1093/bioinformatics/bty895

Zoller R, Schulz C. 2012. The *Drosophila* cyst stem cell lineage: partners behind the scenes? *Spermatogenesis* **2:** 145–157. doi:10.4161/spmg.21380

Received April 19, 2025; accepted in revised form October 9, 2025.